Tumor Suppressor ARID1A Deficiency Impairs DNA Damage Checkpoint and Sensitizes Cells to PARP Inhibitors

Jianfeng Shen[1], Yang Peng[2], Li Lan[3], Wei Zhang[1], Lin Yang[1,4], Jeremy Stark[5], Lee Zou[6], Ivan Uray[1], Xiangwei Wu[1], Powel Brown[1], Gordon Mills[2] & Guang Peng[1]

[1]Department of Clinical Cancer Prevention, The University of Texas MD Anderson Cancer Center, Houston, Texas 77030, USA

[2]Department of Systems Biology, The University of Texas MD Anderson Cancer Center, Houston, Texas 77054, USA

[3]Department of Microbiology and Molecular Genetics, The University of Pittsburgh School of Medicine, Pittsburgh, PA 15213, USA

[4]Department of Medical Oncology, Tongji Hospital, Tongji Medical College, The University of Huazhong Science & Technology, Wuhan, Hubei Province 430022, P.R. China

[5]Department of Radiation Biology, Beckman Research Institute of the City of Hope, City of Hope Graduate School of Biological Sciences, Duarte, California, USA

[6]Massachusetts General Hospital Cancer Center, Harvard Medical School, Charlestown, MA 02129, USA

Correspondence should be addressed to G.P. Tel: +1 713 834 6151; Fax: +1 713 834 6397 (gpeng@mdanderson.org).

RUNNING TITLE

ARID1A regulates genomic stability

SUMMARY (120 words)

Chromatin remodeler ARID1A is an emerging tumor suppressor in a broad spectrum of human cancers. Thus it is of paramount clinical importance to understand whether we can exploit ARID1A deficiency therapeutically. In this study we report the function of ARID1A in genome maintenance and its deficiency sensitizes cells to PARP inhibitors. ARID1A is recruited to DNA double strand breaks (DSBs) through its interaction with DNA damage responsive kinase ATR, where ARID1A promotes DSB resection and sustains DNA damage signaling. ARID1A deficiency leads to impaired DNA damage checkpoint, which sensitizes cells to PARP inhibitors. We propose that ARID1A functions as a regulator of DNA damage checkpoint machinery and PARP inhibitors may be beneficial for patients with ARID1A-mutant tumors.

SIGNIFICANCE (120 words)

ARID1A is identified as one the most frequent mutated genes in human cancers in the era of next-generation DNA sequencing. Our study provides mechanistic insights into the function of ARID1A in tumor suppression via preventing genomic instability, which represents a key step to functionalize cancer genomic data. More importantly, our data reveal that loss of ARID1A in certain tumor types may sensitize cancer cells to DSB-inducing treatment such as PARP inhibitors. The data we present here now suggests that the clinical assessment of PARP inhibitors might be extended beyond those with BRCA mutations to a larger group of patients with ARID1A mutant tumors, which may loss DNA damage defense mechanism and exhibit therapeutic vulnerability to PARP inhibitors.

HIGHLIGHTS (85 characters including space)

- Chromatin remodeler ARID1A interacts with ATR and is recruited to DSBs
- ARID1A depletion impairs DSB checkpoint response
- ARID1A promotes DSB end resection and DSB-induced DNA damage signaling
- ARID1A deficiency sensitizes cancer cells to PARP inhibitors

INTRODUCTION

ARID1A (the AT-rich interactive domain 1A gene) is identified as one of the most frequently mutated genes in human cancers by multiple next-generation genomic sequencing studies (Wilson and Roberts, 2011; Wu and Roberts, 2013; Wu et al., 2014). The mutation rate of ARID1A ranges from 10% to 57% in a broad spectrum of cancers including ovarian clear cell carcinoma, uterine endometrioid carcinoma, gastric cancer, hepatocellular carcinoma, esophageal adenocarcinoma, breast cancer, pancreatic cancer, tranitional-cell carcinoma of bladder, renal cancer, waldenstrom macroglobulinemia, pediatric burkitt lymphoma and cholangiocarcinoma (Wilson and Roberts, 2011; Wu and Roberts, 2013; Wu et al., 2014). Furthermore, immunohistochemistry analyses have showed frequent loss of ARID1A expression in these cancers (Wilson and Roberts, 2011; Wu and Roberts, 2013; Wu et al., 2014). Overall, the frequency and patterns of ARID1A mutations strongly indicates that it is an emerging tumor suppressor in human cancers across tumor lineage. However how ARID1A deficiency leads to cancer development and whether we can exploit ARID1A deficiency in human tumors therapeutically remain to be unanswered questions.

ARID1A, also known as BAF250a, is a subunit of an evolutionarily conserved chromatin remodeling complex SWI/SNF (Wang et al., 2004a; Wang et al., 2004b). SWI/SNF

complex is evolutionarily conserved in all eukaryotes (Roberts and Orkin, 2004). It uses the energy of ATP hydrolysis to reposition, eject, or exchange nucleosomes, which modulate DNA accessibility to cellular processes involved in chromatin structure such as transcription, DNA replication and DNA repair (Imbalzano et al., 1994; Kwon et al., 1994; Wang et al., 2007). SWI/SNF complex contains multiple subunits, where BRG1/BRM, SNF5, BAF155 and BAF170 function as core subunits with ATPase catalytic activity (Phelan et al., 1999). ARID1A, as well as its paralog ARID1B, functions as a variant subunit, which is thought to associate with SWI/SNF core subunits and provide target specificity (Roberts and Orkin, 2004; Wang et al., 2004a; Wang et al., 2004b). From our proteomic analysis to identify interacting proteins with a DNA damage responsive kinase ataxia telangiectasia and Rad3-related (ATR), we surprisingly found that ARID1A is a previously unknown binding partner of ATR. Recent cancer genomic studies reveal that human cancers result in large part from the accumulation of multiple genetic alterations including mutations, deletions, translocations and amplifications (Vogelstein et al., 2013). Thus, our proteomic result raised an intriguing question whether ARID1A plays a role in maintaining genomic integrity through its interaction with ATR, which could be crucial for preventing initiation and development of a wide spectrum of human cancers.

ATR is a member of the phosphoinositol 3-kinase-like kinase (PIKK) family. Along with kinase ataxia telangiectasia-mutated (ATM), ATR functions as a central regulator to control DNA damage-induced phosphorylation cascade (Ciccia and Elledge, 2010), which forms the most important DNA damage response (DDR) program to detect, signal

and repair damaged DNA, and to coordinate cell cycle checkpoint activation and cell death pathways such as apoptosis and senescence (Ciccia and Elledge, 2010; Harper and Elledge, 2007; Jackson and Bartek, 2009). In DDR, ATM and ATR-mediated signaling pathways have both interdependent and distinct roles. In general ATM and ATR respond to different types of DNA damage: ATM is activated by double-strand DNA breaks (DSBs), whereas ATR responses to single-strand DNA breaks (SSBs) (Zhou and Elledge, 2000). However the ATM- and ATR-activating DNA lesions are inter-convertible. DSBs activate ATM but can also activate ATR as a consequence of DSB end resection, which generates single-stranded region (Adams et al., 2006; Jazayeri et al., 2006; Myers and Cortez, 2006). Whereas SSBs activate ATR due to stalled replication forks, which can be cleaved by nucleases and cause DSBs formation (Schlacher et al., 2011). Once activated by DNA lesions, ATM and ATR phosphorylate a variety of common substrates. The overlapping and redundancy of these substrates provide an extensive crosstalk between ATM and ATR pathways, which allow them to function in a collaborative manner to maintain genomic stability (Matsuoka et al., 2007). However, unlike ATM, ATR is essential for cell survival (Brown and Baltimore, 2000), supporting the functional importance of ATR for multiple genome maintenance programs including checkpoint activation, DNA repair and DNA replication at various stages of cell cycle progression. For example, in S phase, ATR regulates replication initiation, replisome stability, replication fork restart (Cimprich and Cortez, 2008). In G2 phase, ATR prevents premature mitotic entry in the presence of damaged DNA via the G2 checkpoint (Brown, 2003; Cortez et al., 2001). However, it remains to be a key question: how ATR signaling is regulated for its versatile roles in DDR? One possible mechanism is that ATR

interacting proteins provide fine-tuned regulatory elements in determining temporal and special functions of ATR in DDR. Therefore we conducted a proteomic analysis to systematically identify ATR interacting proteins. Among many known ATR binding proteins such as ATRIP, we identified ARID1A as a new interacting partner of ATR.

In this study, we found ARID1A is recruited to DSBs via its interaction with ATR. In response to DNA damage, ARID1A is required for processing DNA DSB ends to generate RPA-coated single strand DNA (ssDNA), a key step for ATR activation in response to DSBs potentially through altering chromatin environment at DNA breaks and allowing for DSB end resection. Consequently, loss of ARID1A leads to impaired checkpoint activation and DNA repair of DNA DSBs, which sensitizes cells to DSBs-inducing DNA damage such as radiation and poly(ADP-ribose) polymerase (PARP) inhibitors. Thus, our results provide biological insights into the function ARID1A as a tumor suppressor in human cancers and a mechanistic basis for targeting ARID1A-deficient tumors.

RESULTS

ARID1A is Recruited to DNA Breaks via Its Interaction with ATR.

In order to explore the regulatory mechanisms for the functions of ATR in DDR, we conducted immunoprecipitation (IP) assay to purify ATR-associated protein complexes and then subjected to silver staining and mass spectrometry analysis (Figure 1A). Among many known ATR binding proteins such as ATRIP, we found ARID1A as a new binding partner of ATR (Figures 1A and S1). To confirm the result from proteomic study, we

performed reciprocal IP with V5-tagged ARID1A (Figure 1B) and endogenous IP analyses (Figure 1C), showing that ARID1A is indeed an ATR interacting protein. Given the important role of ATR in DNA damage response, next we tested whether ARID1A is recruited to DNA breaks. Current available ARID1A antibodies could not detect the ionizing induced foci formation (IRIF) of ARID1A at DNA breaks. Thus we used chromatin immunoprecipitation (ChIP) assay to examine whether ARID1A is recruited to the proximity of a single site-specific I-SceI-induced DSB (Figure 1D) as previously described (Peng et al., 2009; Pierce et al., 1999). Interestingly, we found that ARID1A was enriched at the chromatin region close to DSB induced by I-SceI. To facilitate the visualization of the recruitment of ARID1A to the DNA lesions, we used a light activation system (Killer Red System) to further confirm the localization of ARID1A at DSBs upon laser activation (Carpentier et al., 2009; Lan et al., 2010; Pletnev et al., 2009). As shown in Figures 1E and S2, EGFP-tagged ARID1A predominantly localized in the nucleus. Upon laser activation, ARID1A showed a specific enrichment at the DNA damage site, which was co-localized with Killer Red signals. These findings reveal that ARID1A interacts with ATR and is recruited to DSBs. We then set out to determine whether the recruitment of ARID1A to DSBs is dependent on its interaction with ATR.

First, we transiently knockdown ATR and examined the recruitment of ARID1A to DSB via I-SceI-based ChIP analysis. As shown in Figure 2A, in ATR knockdown cells, the recruitment of ARID1A to DSBs was significantly reduced. This result suggested that ATR is required for recruiting ARID1A to DNA lesions. Second we examined whether DNA damage signaling induced by DDR kinases ATM and ATR is required for the

recruitment of ARID1A to DSBs. We treated cells with chemical inhibitors of ATM or ATR. The effectiveness of these inhibitors on blocking DNA damage signaling was shown in Figure 2B by using their downstream phosphorylation targets. In this experiment, we found that ATM inhibitor could remarkably decrease the recruitment of ARID1A to DSBs (Figure 2B). However ATR inhibitor has less impact on regulating its recruitment compared to ATM inhibitor, although ATR knockdown significantly reduced the recruitment of ARID1A to DSBs (Figures 2A and 2C). Consistent with previous findings that ATR recruitment to DSBs requires ATM (Adams et al., 2006; Jazayeri et al., 2006; Myers and Cortez, 2006), these data suggest that the interaction between ARID1A and ATR and proper DNA damage signaling initiated by ATM are required for ARID1A recruitment.

To gain molecular details in ARID1A-ATR interaction and the recruitment of ARID1A to DSBs, we first used two deletion constructs to test whether ARID1A binds to ATR through its N-terminal half or its C-terminal half. As shown in Figure 2C, C-terminal ARID1A had a strong binding affinity to ATR, whereas N-terminal ARID1A could not pulldown ATR although N-terminal ARID1A had a comparable expression level as full-length protein did. This result suggested that the domains required for ATR interaction are located in the C-terminal half of ARID1A. Then, we generated deletion mutants of the C-terminal half of ARID1A to further pinpoint the regions mediating its interaction with ATR. By using these constructs, we found that regions from 1800-1900 aa and 2100-2200 aa at the C-terminal half of ARID1A were essential for its interaction with ATR (Figures 2D and 2F).

ARID1A is frequently mutated in human cancers. As expect for inactivating mutation for a tumor suppressor gene, the mutations were found to distribute throughout the gene and included nonsense and missense changes, out-of-frame and in-frame small insertions and deletions. To determine the pathological significance of patient-derived mutations, we searched for ARID1A mutations in its ATR-interacting domain and we found that c5548delG is a mutation hotspot, which is commonly identified in multiple cancers including colon cancer, gastric cancer and pancreatic cancer (Jones et al., 2012). Thus, we tested whether this mutation abolished ARID1A-ATR interaction. As shown in Figures 2E and 2F, ARID1A (5548delG) mutated C-terminal half ARID1A failed to bind to ATR. In contrast, another patient-derived mutant ARID1A (5715delA), which was not localized to ARID1A-ATR interacting regions, could interact with ATR at the same expression level as ARID1A (5548delG). To confirm that the ARID1A-ATR interaction is required for its recruitment to DSBs, we determined the binding capability of the full-length V5-tagged ARID1A (5548delG) mutant to I-SceI-induced DSBs. We found that indeed mutant ARID1A lack of ATR interacting capacity could not be recruited to the proximal regions of DSBs as efficiently as wild-type ARID1A (Figure 2G). Moreover, we examined the recruitment of EGFP-tagged wild-type and mutant ARID1A to DNA lesions by using Killer-Red mediated light activation system. As expected, mutant ARID1A reduced binding efficiency to damaged DNA (Figure 2H).

Collectively, these data show that ARID1A interacts with ATR via its C-terminal region, which mediates its recruitment to DSBs. A frequent mutation c.5548delG identified from

cancer patients is located in ARID1A-ATR interacting domain, which impairs the recruitment of ARID1A to DSBs. Next we asked whether ARID1A deficiency impairs cellular response to DNA damage.

ARID1A Is Required for Proper G2/M DNA Damage Checkpoint

We used isogenic HCT116 cell lines with wild-type ARID1A and a knock-in mutant ARID1A (Q456*/Q456*), which abolishes ARID1A expression due to an early stop codon, as our model system. We first examined the cell cycle distribution at different time points after IR. As shown in Figure 3A, one hour after IR, control cells started to accumulate at G2/M checkpoint, which led to a significant increase of cells at G2/M phase at 4 hrs and 8 hrs after IR, suggesting ARID1A-depleted cells showed a weaken G2/M checkpoint activation (Figure 3). Sixteen hours after IR, while control cells still maintained a large proportion of cells arrested at G2/M checkpoint, ARID1A-depleted cells exhibited a markedly reduced percentage of cells at G2/M checkpoint with a significant increase of cells in G1 phase (Figure 3A). These results indicate that ARID1A deficiency leads to an impaired G2/M checkpoint initiation and maintenance. To confirm these results, we used phospho-Histone H3 staining to measure the fraction of mitotic cells after IR in ARID1A-depleted cells. Without IR treatment, there was no apparent difference in the percentage of mitotic cells after ARID1A depletion (Figure 3B). After exposure to IR, the percentage of mitotic positive cells was significantly reduced and started to recover 16 h after IR (Figure 3B). In contrast, ARID1A-deficient cells showed a slower decrease of mitotic cells in early time points after IR and a significant increased number of cells re-entrying into mitosis at 16h after IR, suggesting a defective G2/M

checkpoint initiation and maintenance (Figure 3B). In accord with this, as shown in Figure 3C, ARID1A depletion led to a remarkable increase in cumulative mitotic reentry after IR exposure as measured by paclitaxel treatment, which blocks the mitotic exit. Defective G2/M checkpoint maintenance was not due to the differential response to paclitaxel, since we observed a comparable block in mitotic accumulation when analyzed without IR (Figure 3C). Effective depletion of ARID1A expression in ARID1A null cells was shown in Figure 3D. These data therefore indicated that ARID1A deficiency significantly impairs G2/M checkpoint initiation and maintenance. As ARID1A is a subunit of SWI/SNF complex, we then asked whether the chromatin remodeling activity of SWI/SNF complex is required for G2/M checkpoint response. We knockdown the core catalytic subunit BRG1 or BRM in U2OS cells (Figure S3) and found that BRG1 deficiency led to a similar increase of mitotic cells 16 h after IR compared to ARID1A knockdown cells (Figure 3E). This result suggested that ARID1A associated BRG1-SWI/SNF complex is required for maintaining G2/M cell cycle arrest after DSBs.

ARID1A Deficiency Impairs ATR Activation-Induced by DSBs

Having observed a defective DNA damage checkpoint in ARID1A-deficient cells, we further examined whether ARID1A deficiency impairs DNA damage checkpoint signaling pathway. We treated cells with IR and examined the activation of CHK1, a key G2/M checkpoint regulator. In ARID1A-depleted cells, we found reduced CHK1 (S317) phosphorylation in response to IR particularly at late time point (8hrs after IR) (Figure 4A). In response to DSBs, CHK1 (S317) is a specific phosphorylation target site for ATM and ATR. Thus we examined whether ARID1A deficiency affects ATM and/or

ATR activation. In response to damaged DNA, ATM (S1981) and ATR (T1989) become autophosphorylated, which are recognized as markers for the activation of their kinase activity (Jazayeri et al., 2006; Kozlov et al., 2006; Liu et al., 2011; Nam et al., 2011). Therefore, we examined ATM and ATR autophosphoryaltion in response to IR in ARID1A-depleted cells. As shown in Figure 4B, ARID1A deficiency remarkably reduced ATR activation in response to IR. However its depletion did not have any significant effect on regulating ATM activation and the recruitment of ATM to DNA damage sites (Figures 4C and S4). Previous findings have shown that the G2/M checkpoint is impaired in the absence of ATR (Brown and Baltimore, 2000). Thus, our data suggest that ARID1A depletion may impair ATR activation in response to DSBs and thereby affect checkpoint signaling (Figure 3).

In general, DSB ends are the preferred substrate for ATM binding, which activates ATM first and then ATR is activated to sustain ATM-initiated signaling (Harper and Elledge, 2007). Therefore, we examined the effect of ARID1A deficiency on the dynamic of H2AX phosphorylation, which is directly targeted by both ATM and ATR. As we expected, chromatin binding of γ-H2AX was significantly reduced at 8 hrs compared to 4 hrs after IR, indicating the impairment of sustained γ-H2AX formation (Figure 4D). To confirm this result, we tested whether ARID1A deficiency reduces γ-H2AX foci formation, which directly reflects the accumulation of γ-H2AX at DSBs. As shown in Figure 4E, γ-H2AX foci formation was significantly reduced at later time points after IR. In addition, we examined the foci formation of DNA damage responsive protein 53BP1. 53BP1 is a key adaptor protein in checkpoint response, whose recruitment to DSBs is

dependent on the protein platform assembled by γ-H2AX formation (Panier and Boulton, 2014). Consistent with the reduced γ-H2AX foci formation at 8 hrs after IR, 53BP1 foci formation was remarkably reduced (Figure 4F). As shown in Figure S5, we used comet assay to determine the presence of DSBs. ARID1A-depleted cells had a comparable level of DSB formation after IR, suggesting that reduced γ-H2AX and 53BP1 foci formation was not due to the reduced level of DSBs. Collectively, these results indicate that ARID1A deficiency impairs ATR-mediated signaling in response to DSBs, which is required for sustaining DSB-induced DNA damage signaling.

ARID1A Deficiency Impairs DSB End Resection for Initiating DSB-induced ATR Signaling

Next we sought out to determine the molecular mechanism underlying the defective ATR activation induced by DSB in ARID1A-deficient cells. In response to DSBs, ATM is directly activated by the MRN (MRE11-RAD50-NBS1) complex, which is required to recruit ATM to DSBs (Berkovich et al., 2007; Falck et al., 2005; Lee and Paull, 2005), whereas the recruitment and activation of ATR to DSBs require the formation of RPA-coated SSBs, which arises from 5'-3' resection of DSB end (Cortez et al., 2001; Zou and Elledge, 2003). Therefore, we ask whether ARID1A depletion affects the process of DSB end resection, which leads to reduced efficiency of ATR activation. First, we examined phosphorylation of ssDNA-binding protein RPA in ARID1A depleted cells, as an indicator of DSB resection efficiency (Polo et al., 2012). As shown by western blot analysis (Figure 5A), IR-induced phosphorylation of the RPA2 subunit (Ser-4 and Ser-8) was significantly reduced after ARID1A depletion. In contrast, ARID1A deficiency did

not affect RPA phosphorylation in response to replication stress stimuli HU and UV treatment, although both HU and UV can induce much stronger RPA phosphorylation than IR did (Figure 5B). This result suggested that ARID1A specifically affect DSBs-induced formation of ssDNA. To confirm this observation, we used immunofluorescent staining to detect this phosphorylation event at DNA damage sites. Notably, ARID1A depletion markedly reduced formation of p-RPA (Ser4/Ser8) foci formation, which indicated RPA accumulation and the impaired the ssDNA formation at DSBs (Figure 5C). Furthermore, we tested the effect of ARID1A loss on the chromatin environment around DSBs. We examined the histone H3 occupancy at I-SceI-induced DSB site by ChIP assay. We found that H3 deposition was not altered in ARID1A-depleted cells before DNA damage (Figure 5D). However, H3 occupancy was much higher in ARID1A-depleted cells after I-SceI-induced DSBs. These data support an impaired DSB end resection due to loss of ARID1A, suggesting that ARID1A is required to create a favorable chromatin environment for efficient DSB end resection. Moreover we determined whether ARID1A depletion affects DSB repair via homologous recombination (HR) and single strand annealing (SSA), which represent the repair mechanisms required DSB end resection (Figure S6). In line with our findings that ARID1A is required for efficient DSB end resection, we found that ARID1A knockout indeed impaired HR repair and SSA repair efficiency (Figures 5E and 5F). In addition, to exclude the potential impact of ARID1A depletion on gene transcription regulation, we examined the key molecules involved in DDR and DSB resection in ARID1A-depleted cells, we did not observe any apparent reduced protein expression levels (Figure S7). Together these data suggest that initial DSB end resection resulted from ATM-MRN

complex-dependent signaling recruits ATR, which in turn recruits ARID1A to promote DSB end resection and ATR activation and thereby augment DSB-induced DNA damage signaling.

ARID1A Deficiency Sensitizes Cells to DNA Damage-Inducing Agent PARP Inhibitors

Poly(ADP-ribose) polymerase inhibitors are recently developed anti-cancer drugs targeting a key enzyme PARP1 involved in repairing DNA SSBs (Bryant et al., 2005; Farmer et al., 2005). PARP inhibitor treatment causes failure of SSB repair, which can be converted into DSBs when DNA replication forks stall and collapse at the persistent SSB lesions (Bryant et al., 2005; Farmer et al., 2005). Therefore, PARP inhibitors are highly selectively lethal to cells lacking BRCA1 or BRCA2, two genes in repairing DSBs, while they exhibit minimal toxicity to normal cells and less therapeutic effects in cancer cells without DSB repair deficiency(Bryant et al., 2005; Farmer et al., 2005). We found that ARID1A-depleted cells exhibit a significant G2/M checkpoint defect in response to DSBs, which may lead to an insufficient cell cycle arrest for DSB repair. In addition, ARID1A deficiency impaired DSB repair process through both HR and SSA mechanisms. Based on these observations, we reasoned that ARID1A deficiency may provide a therapeutic vulnerability to DSBs induced by PARP inhibitors. Therefore, we tested this hypothesis in a variety of isogenic models with multiple PARP inhibitors, which are currently used in clinical trials. First, we knockdown ARID1A in two immortalized normal breast epithelial cell lines MCF10A and HMEC and then we treated cells with different PARP inhibitors Olaparib, Rucaparib and Veliparib. As shown in

Figures 6A and 6B, PARP inhibitors selectively inhibited the survival of cell lacking ARID1A expression. In the next experiment, we tested whether ARID1A depletion sensitizes cancer cells to PARP inhibitor treatment in colon cancer cell line HCT116 and breast cancer cell line MDA-MB-231. We treated cancer cells with Olaparib and BMN673, a potent PARP inhibitors reported from most recent studies. As expected, ARID1A knockdown cells showed a remarkably reduced number of colony formation in the presence of PARP inhibitors (Figure 6C). It is worthy of noting that in addition to the reduced number of colony, BMN673 treatment also reduced the average of size of colony formation compared to Olaparib treatment, suggesting its strong anti-cancer cell survival effect. In line with these findings, ARID1A-depleted cells showed significantly enhanced apoptosis after exposure to PARP inhibitors in MDA-MB-231cell line (Figures 6D, 6E) and in HCT116 cell line (Figure F). To further confirm the function of ARID1A in DNA damage response is responsible for sensitizing ARID1A-deficient cells to PARP inhibitors, we reconstituted ARID1A knockout-HCT116 cells with wildtype or mutant ARID1A (c.5548delG), which cannot be recruited to the DSB sites. As shown in Figure 6G, mutant ARID1A was not able to rescue enhanced PARP inhibitor-induced apoptosis in ARID1A-depleted cells. In contrast, expression of wild-type ARID1A significantly reduced apoptosis after PARP inhibitor treatment, although the rescue was partial, which was likely due to the transient reconstitution of ARID1A wildtype construct in these cells. This result suggested that indeed the recruitment of ARID1A to DSBs is essential for its function in regulating DDR.

Compared to Olaparib and Veliparib, Rucaparib and BMN673 showed stronger effects on inhibiting cell survival and inducing apoptosis in ARID1A-deficient cells. Thus we examined whether Rucaparib and BMN673 exhibit a dose-dependent induction of apoptosis in ARID1A-depleted cells. As shown in Figure 6H, both drugs could induce a stronger apoptotic effect in ARID1A-depleted cells in a dose-dependent manner compared to control cells. Consistent with previous findings indicating BMN673 as a potent PARP inhibitor (Cardnell et al., 2013; Shen et al., 2013), it significantly induced apoptosis in ARID1A-deficient cells at much lower concentrations than Rucaparib. Therefore, in the next step, we tested the selective antitumor effects of BMN673 against ARID1A-deficient cancer cells in vivo.

PARP Inhibitor BMN673 Oral Administration Selectively Inhibits ARID1A-Deficient Tumors in Xenograft Models

We xenografted ARID1A-deficient breast cancer cells MDA-MB-231 and ARID1A-depleted colon cancer cells HCT116 into nude mice and treated animals with BMN673. Oral administration of BMN673 (once a day dose of 0.33 mg/kg) significantly inhibited the growth of ARID1A-deficient xenografts in mice (Figures 7A, 7B and 7D), whereas it had no apparent antitumor effect on ARID1A-wildtype xenografts (Figures 7A, 7C and 7E). HCT116 cells grew xenograft tumors much faster than MDA-MB-231 cells. Due to the significant tumor burden in the untreated group, HCT116 xenograft mice were treated with BMN673 for 16 days. After 1 week treatment, BMN673 started to show a remarkable selective antitumor efficacy in ARID1A-depleted HCT116 cells and this antitumor effect became more significantly after 16-day treatment (Figure 7B). MDA-

MB-231 xenografts were treated with BMN673 for 30 days, where BMN673 significantly inhibited tumor growth in ARID1A-deficient cancer cells (Figure 7D). In both xenograft models, at the end of scheduled treatment, growth from ARID1A-deficient xenografts was suppressed by BMN673 when compared to vehicle-treated xenografts (Figure 7F). Conversely BMN673 did not have a similar effect on the growth of ARID1A wild type xenografts (Figure 7F). Furthermore, we analyzed the expression of apoptosis marker cleaved caspase 3 and DNA damage response marker phosphorylated CHK1 in xenograft tumor tissues. As expected, ARID1A-deficient cancer cells failed to response BMN673-induced DNA damage appropriately with a much lower expression level of p-CHK1 than control cells with wild type ARID1A (Figure 7G). In accord with this observation, ARID1A-deficient tumor cells has an enhanced apoptosis induced by BMN673 treatment (Figure 7G). In summary, our study provides data to suggest that targeting the defective DNA damage response could be beneficial for cancer patients with ARID1A-deficient tumors. PARP inhibitors may be a useful drug to treat these patients.

DISCUSSION

Our study indicates that ARID1A interacts with ATR and is recruited to sites of DNA damage in an ATR-dependent manner and thereby promotes effective DNA DSB end resection, a process required for promoting ATR-dependent signaling from DSB sites and repair of DSBs through homologous recombination pathways. In light of these findings, our in vitro and in vivo data further show that PARP inhibitors can selectively target ARID1A-deficent cells. Collectively our results provide mechanistic insights into how

ARID1A suppresses tumorigenesis and how we might exploit ARID1A deficiency therapeutically.

ARID1A was identified as one the most frequent mutated genes in human cancers from genome-wide DNA sequencing studies (Wu and Roberts, 2013; Wu et al., 2014). Later functional studies showed that restoration of ARID1A expression in a variety of cancer models can repress cancer cell proliferation and xenograft tumor growth, suggesting ARID1A functions as a tumor suppressor (Wu and Roberts, 2013; Wu et al., 2014). Multiple studies have pointed tumor suppressor roles for ARID11A in regulating a transcriptional program of a proper cell cycle progression. In an ovarian cell line model, ARID1A-associated SWI/SNF complexes is found to be recruited to p21 promoter through interaction with p53 (Guan et al., 2011). In a pre-osteoblast cell line model, ARID1A is required for differentiation-associated cell cycle arrest through repressing E2F-responsive promoters and c-myc promoter, which leads to p21 induction(Nagl et al., 2005) . Using Drosophila neuroblasts, SWI/SNF component Osa (ARID1) prevents tumorigenesis by inducing a transcriptional program that initiates temporal patterning, limits self-renewal and prevents dedifferentiation (Eroglu et al., 2014). Interestingly, our study report a new role of ARID1A-associated SWI/SNF complexes in preventing genomic instability. Specifically in response to DSBs, ARID1A is required for overcoming chromatin barrier for DSB end resection, which allows for generating RPA-coated ssDNA and efficiently activating ATR signaling to arrest cell cycle at G2/M checkpoint. Thus, our results indicate that ARID1A, in addition to its role as a transcription ‘gatekeeper’ in regulating normal cell cycle transition, in the stress

condition with the presence of DSBs, it can also function as a 'caretaker' to maintain genomic integrity. Consistent with this 'caretaker' role of ARID1A identified in our study, previous studies also found that knockdown SWI/SNF core component BRG1 or BRM can affect DNA repair pathways and DNA damage response (Wilson and Roberts, 2011). Notably, in the absence of DNA damage stress, ATPase activity of BRG1, the core subunit of SWI/SNF complex is found to be required for localization of topoisomerase II alpha (TOP2A) to genome and thus plays a role in decatenating newly replicated sister chromatids and maintaining proper chromaosome segregation in mitosis (Dykhuizen et al., 2013). These findings together with our study support that tumor suppressor ARID1A is an emerging epigenetic regulator of genome stability, which may explain why ARID1A mutations are frequently observed in multiple lineages of human cancers.

As a new regulator of ATR signaling , our results show that ARID1A is recruited to DSBs via its interaction with ATR and this recruitment in turn is required for promoting efficient ATR activation. It is well-known that ATR is activated by RPA-coated ssDNA (Zou and Elledge, 2003). Moreover, RPA-ssDNA is not only a quantitative signal for ATR-ATRIP recruitment but also a length-dependent platform that promotes ATR activation (Cimprich and Cortez, 2008; Liu et al., 2011). Thus, in response to DSBs, DNA end resection to generate ssDNA becomes a key regulatory step for efficient ATR activation. Recent studies have characterized a two-stage model of DSB end resection. In this model, initial limited resection is mediated by MRE11-RAD50-NBS1 (MRN) sensor complex and CtBP-interacting protein (CtIP) (Clerici et al., 2005; Gravel et al., 2008;

Limbo et al., 2007; Sartori et al., 2007) , which subsequently leads to longer-range resection involving EXO1, BLM and DNA2 (Budd and Campbell, 2009; Mimitou and Symington, 2008; Nimonkar et al., 2011). However little is known how the switch from initial to long resection is controlled, which contributes to initial ATR recruitment to persistent ATR activation at DSBs. Our results suggest that ARID1A may function as an epigenetic switch to coordinate this two-stage resection process. In response to DSBs, MRN and CtIP may generate initial ssDNA for recruiting ATR. Thereby ARID1A is recruited to DSBs via its interaction with ATR and thus promotes a favorable chromatin environment for long resection, which further promotes ATR activation and ATR-dependent signaling in response to DSB. It is worthy of noting that we observed predominant defect in G2/M checkpoint, however we only found mild defects in HR repair and SSA repair, which are also dependent on DSB end resection. There are two possibilities to explain this phenomenon. First, additional factors may participate in resection during DSB repair process. Previous studies have shown that SWI/SNF component SMARCAD1 is a nucleosome remodeling enzyme required for resection of DSB end during DNA repair (Chen et al., 2012; Costelloe et al., 2012). It is possible that a different sub-complex of SWI/SNF may contribute to DSB repair, which alleviates the defective resection in the absence of ARID1A during the repairing process. Second, in our study we observed the reduced levels of 53BP1 foci at the late time point of checkpoint activation (8hrs after IR). 53BP1 is a mediator of DSB signaling, which provides a molecular scaffold to recruit DSB-responsive proteins and is required for G2/M checkpoint (Panier and Boulton, 2014). In addition, 53BP1 is also required to protect DSBs from end resection (Panier and Boulton, 2014). The impaired 53BP1

accumulation at DSBs in ARID1A-depleted cells may relieve the block for resection at late time point after IR and led a mild defect in repair compared to checkpoint defect. In summary our study shows that tumor suppressor ARID1A appears to be an epigenetic component of checkpoint machinery through regulating ssDNA generation at the DSB end, which ensures a proper checkpoint response by controlling the ATR activation.

In addition to providing biological insights into the function of ARID1A in genome maintenance, our study further show that PARP inhibitors can selectively inhibit ARID1A-deficient cells both in vitro and in vivo models we tested. As target therapeutic drugs, monotherapy of PARP inhibitors is found well-tolerant in patients, however with minimal therapeutic effects without specific genetic defects such as BRCA1/BRCA2 mutations (Ellisen, 2011). Thus, our study provides a mechanistic rationale for testing the efficacy of PARP inhibitors in ARID1A-deficient tumors. It is worthy of noting that we found that ARID1A mutation 5715delA can interact with ATR whereas mutation 5548delG cannot bind to ATR. This result suggests that not all ARID1A mutations will result in defective DNA damage response. Therefore it is imperative to treat ARID1A-mutant tumor based on the biological significance of its mutation.

Moreover, specific inactivating mutations in several other SWI/SNF subunits have also been frequently found in various human cancers including PBRM1, ARID2, ARID1B, BRG1, SNF5 and BRD7 (Wilson and Roberts, 2011). However mutations in different SWI/SNF subunits lead to distinct cancer spectrum (Wilson and Roberts, 2011). For example, SNF5 mutations are found in nearly all malignant rhabdoid tumors (Roberts and

Biegel, 2009), while PBRM1 mutations are identified in 40% of renal cancers (Varela et al., 2011). Consistent with these observations, genetic knockout mouse model with individual SWI/SNF subunit exhibits distinct phenotypes (Roberts and Orkin, 2004; Wilson and Roberts, 2011). These findings support that individual subunits may have distinct tumor suppressor roles in specific tissue contexts. Given the diverse combination and interactions of subunits in a particular SWI/SNF complex, it is possible that ARID1A may have distinct effects on tumorigenesis in different tissues through both transcription-dependent and –independent mechanisms. Recently ARID1A/B are found to contain putative E3 ubiquitin ligase activity. It is likely it may function as a regulator of ubiqutination process, which adds an additional complexity of ARID1A's function (Li et al., 2010). Therefore, it might be expected that ARID1A may have distinct mechanisms for tumor suppression in a tissue-dependent manner. It is of interests to investigate to what extent ARID1A deficiency leads to defective checkpoint activation in different cancer tissues. The answer to this question will be instrumental to guide therapy with DNA damage inducing agent such as PARP inhibitors. It has been found that ARID1A mutations cooperate with activation of PI3K/AKT pathway in promoting tumorigenesis (Wu and Roberts, 2013; Wu et al., 2014). A most recent study showed that depletion of ARID1B reduces survival of ARID1A mutant cancer cells (Helming et al., 2014). Thus it is possible to explore mechanism-based combination treatment by using PARP inhibitors with PI3K/ATK inhibitors or strategies targeting ARID1B, which may provide new therapeutic avenues for patients with ARID1A mutated tumors.

EXPERIMENTAL PROCEDURES

Cell Culture and Plasmids

HCT116 parental and ARID1A knockout (Q456*/Q456*) cell lines were purchased from Horizon Discovery Ltd and were maintained according to the manufacturer's instruction. U2OS cells and breast cancer cell lines were purchased from the American Type Culture Collection. U2OS cells were maintained in McCoy's 5A medium (Cellgro) supplemented with 10% FBS with glutamine, penicillin, and streptomycin. MDA-MB-231 breast cancer cells were grown in RPMI 1640 medium supplemented with 10% FBS. HMEC were grown in HuMEC medium with the addition of growth supplement. MCF10A cells were maintained in mammary epithelial growth medium (Clonetics), a proprietary serum-free medium containing insulin, hydrocortisone, epidermal growth factor, and bovine pituitary extract. Cells were incubated at 37°C in a humidified incubator with 5% CO2.
The pCDNA6-V5-ARID1A and its deletion form 1-1758aa and 1759-2285aa were kindly provided by Dr. Ie-Ming Shih, Johns Hopkins University School of Medicine. The EGFP-ARID1A and its mutant forms were generated from the company Custom DNA Constructs. Other mutations were generated by QuickChange II Site-Directed Mutagenesis Kit (Stratagene). The identity of all plasmids was confirmed by sequencing at the M.D. Anderson Cancer Center DNA Core Sequencing Facility.

Antibodies and Reagents

Anti-ARID1A (1:500) and anti-RPA (1:1,000) antibody was purchased from Bethyl Laboratories. Anti-V5 (1:1,000) antibody was purchase from Life Science Technology. Anti-□H2AX (1:1,000) antibody was purchased from Millipore. Anti-53BP1 (1:2,000)

antibody was purchased from Novus Biologicals. Anti-ATR (1:500) antibody was purchase from Santa Cruz Biotechnology. Apoptosis detection kit was purchased from BD Biosciences. Anti-ATRIP (1:1,000), p-ATM (1:500), p-Chk1 (1:500), p-Chk2 (1:500), p-H3 (1:500) antibodies were purchased from Cell Signaling Technology. Anti-Tubulin and anti-β-actin were purchased from Sigma. The PARP inhibitors Olaparib, Veliparib, Rucaparib and BNM673 were purchase from Selleckchem. The silver staining kit was purchased from Thermo Scientific.

KillerRed system

KillerRed (KR) is a light-stimulated ROS-inducer fused to a tet-repressor (tetR-KR), which binds to a TRE cassette (~ 90 kb) integrated at a defined genomic locus in U2OS cells (U2OS TRE cell line) (40). KR facilitates the formation of oxygen radicals and superoxide through the excited chromophore (41, 42) to induce DNA damage. By targeting the expression of KR to one specific genome site, we can visualize the recruitment of proteins at genetic loci. To activate KR, tetR-KR was exposed to 559 nm laser light for 50 scans (over a total of 10 s) at a power rate of 1 mW/scan (equal to 50 mW). At "the KR-TRE array" induced localized damage, we have detected γ-H2AX at the site of tetR-KR but not tetR-monomer cherry (tetR-mcherry) after laser light exposure (unpublished data). For bleaching KR, a 559 nm laser (1 mW/scan) in a selected area was used (FV1000 SIM Scanner set with 405 nm laser diode, Cat. F10OSIM405, Olympus). The dose that was delivered to the KillerRed spot was calculated based on the pixel size, the pixel size for irradiation is (0.138 um/pixel) and the dwell time per pixel is (8 us/pixel). The irradiation is at 1.0 mW (1.0 mJ/s). With a dwell time of 8 us/pixel, this

irradiates each pixel with 8.0 nJ/pixel/scan. Multiplying by the number of scans gives the total energy per pixel.

Flow cytometric analyses

Cell cycle profiles were measured by flow cytometry using propidium iodide (PI). Briefly, HCT116 or U2OS cells were plated at 3×105 cells/plate in 60 mm plates 24 hrs prior treatment. Cells were treated by ionizing radiation at various dosages. Taxol (2 μM) was added into the medium 1 hr post radiation and were remained in the medium. At the end of the treatment, cells were trypsinized and collected by centrifugation (1,000 RPM for 5 min RT). Cell pellets were resuspended in PBS and fixed in 70% ethanol for 1 hr at 4°C. After being washed twice with PBS, cells were incubated at RT 30 min in dark with PI staining solution containing 50 μg/ml PI (Calbiochem, La Jolla, CA), 20 μg/ml RNase A (Novagen) and 0.05% Triton X-100. For p-H3 staining, the cell pellets were incubated with buffer (PBST + 0.1% NP40 + 0.1% Triton X-100) containing Anti-p-H3-Alex673 antibody at 4°C overnight. The cells were washed twice with PBS and stained with PI staining solution. Stained cells were analyzed in Beckman Coulter Gallios flow cytometry using Kaluza Flow Analysis Software.

RNA Interference

ARID1A knockdown was achieved by RNA interference using a lentiviral vector-based MISSION shRNA or siRNA (Sigma). Lentiviral particles corresponding to the MISSION shRNA ARID1A- NM_006015 target set were used, as well as the MISSION nontarget

shRNA control. Specificity and efficacy of the shRNA ARID1A procedure were controlled by western blotting after transduction and puromycin selection in cells. siRNA transfection was conducted using oligofectamin (Life Science Technology) according to the manufacturer's instructions.

Immunoblotting, Immunoprecipitation and Chromatin fractionation

Cells were washed in PBS, and cellular proteins were extracted in 8 M urea lysis buffer plus protease and phosphatase inhibitors (GenDEPOT) for 30 min at 4°C. Lysates were cleared by centrifugation, and proteins were separated by gel electrophoresis. Membranes were blocked in PBS-0.1% Tween 20 (PBS-T)/5% (w/v) milk for 1 hr at room temperature. Membranes were then incubated with primary antibodies diluted in PBS-T/5% (w/v) milk at 4°C overnight. Subsequently, membranes were washed with PBS-T and incubated with horseradish peroxidase secondary antibody (1:2,000) (Jackson ImmunoResearch) diluted in PBS-T/5% skim milk. Membranes were washed in PBS-T, and bound antibody was detected by enhanced chemiluminescence (ECL; GE Healthcare). Immunoprecipitation was performed by incubating lysates from 6 × 106 cells with 1 μg of antibody at 4°C overnight, followed by addition of 20 μl of protein A/G-conjugated agarose beads (GE Healthcare). The precipitates were washed four times with ice-cold PBS, resuspended in 6× Laemmli buffer, and resolved by SDS-PAGE followed by immunoblotting. The preparation of chromatin fractions and western blot analyses, including the conditions for RPA analysis, were performed as described previously (5, 22).

HR and SSA repair assay

The HR and SSA repair assay were performed as described previously (Bennardo et al., 2008; Peng et al., 2009).

Immunofluorescent staining for foci formation

For detection of DNA damage induced foci of γ-H2AX, 53BP1 and p-RPA32, immunofluorescent staining was carried out essentially as described previously (ref). After treatment, cells were subjected to cytoskeleton extraction and stripping, then were fixed in PBS buffered 4% paraformaldehyde. Primary antibodies were incubated at 4°C overnight and secondary antibody Alexa 488-conjugated goat anti-rabbit IgG was incubated for 1 hr at RT. Slides were mounted in medium containing DAPI (Vector laboratories, Burlingame, CA) and analyzed under a fluorescence microscope. At least 50 cells per sample were scored and the foci numbers were calculated.

Chromatin immunoprecipitation (ChIP) assay.

DSBs were induced in cells transfected with control siRNA or ATR siRNA by I-SceI expression. At indicated time points, cells were crosslinked with formaldehyde and ChIPs were performed with an EZ ChIP kit (Upstate) in accordance with the manufacturer's instructions. Cellular lysates were subjected to five sets of sonication on wet ice with a 60 Sonic Dismembrator (Fisher Scientific). Each set consisted of 8 s of sonication separated by 1-min intervals on ice. ARID1A and V5 (5 μl/reaction) antibodies were used for immunoprecipitation. The ChIP primers used to analyse proteins binding at the site of

DSBs were 5′-TACGGCAAGCTGACCCTGAA-3′ (sense) and 5′-GCCCATATATGGAGTTCCGC-3′ (antisense).

Comet Assay

Comet assay was performed as previously described (Peng et al., 2009). Briefly, the presence of DSBs was analyzed by neutral comet assay using the Trevigen's Comet Assay kit according to the manufacturer's instruction. Cells were exposed to 10 Gy IR and subjected to comet analysis at indicated time points. After staining with SYBR green, comet images were captured by fluorescence microscopy. Tail moments (percentage of DNA in tail x tail length) were quantitated for 100 cells/slide by using CometScore Software.

Soft Agar Assay

Cells were resuspended in DMEM containing 0.4% low-melting agarose (Sigma, type VII) and 10% FBS and seeded onto a coating of 0.8% low-melting agarose in DMEM containing 10% FBS. Colonies were scored three weeks after preparation. Colonies larger than 0.1 mm in diameter were scored as positive.

Tumor Growth in Nude Mice

Male athymic nu/nu mice (6–8-week old) were used for all in vivo xenograft studies. Mice were quarantined for at least 1 week before experiments. All animal studies were conducted in compliance with animal protocols approved by the M.D. Anderson Cancer Center Institutional Animal Care and Use Committee. Exponentially growing MDA-MB-

231 ($1x10^6$) or HCT116 ($2x10^6$) cells were implanted subcutaneously at the flank of nude mice. Mice were treated with vehicle or BMN673 (0.33mg/kg) once daily by oral gavage. Tumors were measured every 2 days by calliper to determine tumor volume using the formula [length/2]X[width2]. Each cell line was tested in six different animals.

For immunohistochemistry, tumor tissue samples were fixed in 4% buffered Paraformaldehyde and processed for histopathologic evaluation by paraffin embedding and antibody staining.

Statistical analysis.

All statistical analysis was performed with a two-tailed Student's t-test.

ACKNOWLEDGEMENTS

REFERENCES

FIGURE LEGENDS

Figure 1. ARID1A interacts with ATR and is recruited to DSBs.

(A) Silver staining of the ATR complex separated by SDS-PAGE. The whole cell extracts were prepared from 293T cells. ATR interacting proteins ATRIP and ARID1A are indicated.

(B) Co-IP of ARID1A with ATR analyzed by Western blotting from 293T cells transfected with empty vector V5-Control or V5-ARID1A.

(C) Endogenous interaction between ARID1A and ATR analyzed by Western blotting from 293T cells.

(D) ARID1A is recruited to I-SceI-induced DSBs analyzed by CHIP assay. DRGFP construct containing a cutting site for I-SceI restriction enzyme were stably integrated into U2OS cells as described in Figure S4. Eight hours after I-SceI transfection, ChIP assay were performed. qPCR analyses were used to detect the relative enrichment of ARID1A to the IgG control (Average ± SEM; n=3)

(E) ARID1A is localized at DNA damage sites. GFP-tagged ARID1A and tetR-mcherry or tetR-KR were transfected into U2OS TRE cells. The KillerRed spot was activated with 559 nm laser to induce DNA damage. Representative images after DNA damage by KillerRed activation are shown. Yellow arrowheads: DNA damage sites induced by a tet-repressor fused KillerRed (tetR-KR) expression and light activation as described in Figure S2.

Figure 2. T**he recruitment of ARID1A to DSBs is dependent on its interaction with ATR.**

(A) ATR is required for the recruitment of ARID1A to DSBs. DRGFP-U2OS cells were transfected with control siRNA or ATR siRNA (SMARTpool). Fourty-eight hours later, cells were transfected with I-SceI plasmid. CHIP assay was conducted 8 hrs after I-SceI transfection and qPCR analyses were used to detect the relative enrichment of ARID1A to the IgG control (Average ± SEM; n=3)

(B) The recruitment of ARID1A to DSBs is dependent on ATM/ATR signaling. DRGFP-U2OS cells were pre-treated with ATR inhibitor (ATRi) VE-821 (2μM), and ATM inhibitor (ATMi) KU55933 (10μM) for 30min, and incubated with the inhibitors for additional 8 hrs during I-SceI transfection. ChIP analyses were performed 8 hrs after

induction of DSB by I-SceI transfection. (Left) Phosphorylation of ATM/ATR substrates was detected by indicated antibodies. (Right) qPCR analyses were used to detect the relative enrichment of ARID1A to the IgG control (Average ± SEM; n=3)

(C and D) C-terminal half of ARID1A binds to ATR. 293T cells were transfected with plasmids encoding full length V5-ARID1A (FL) or deletion constructs of V5-ARID1A. Cell lysates were immunoprecipitated using anti-ATR antibody.

(E) Patient-derived mutant ARID1A (5548delG) was unable to bind ATR. 293T cells were transfected with plasmids encoding V5-ARID1A or patient-derived mutants V5-ARID1A (5548delG) and (5715delA). Cell lysates were immunoprecipitated using anti-ATR antibody.

(F) Schematic diagram of ARID1A deletions and mutants.

(G) ARID1A mutant (5548delG) had a reduced enrichment at I-SceI-induced DSBs. DRGFP U2OS cells were transfected with wildtype or mutant V5-ARID1A. Fourty-eight hours later, cells were transfected with I-SceI and 8 hrs later, ChIP assays were conducted with anti-V5 beads. qPCR analyses were used to detect the relative enrichment of ARID1A to the vector control (Average ± SEM; n=3; Student's *t*-test, *<0.01)

(H) The recruitment of ARID1A mutant (5548delG) to DNA damage sites was impaired. (Left) Representative images after DNA damageby KillerRed activation are shown. (Right) Quantitative results represent the mean ± SD of three independent experiments.

Figure 3. ARID1A deficiency impairs G2/M DNA damage checkpoint.

(A and B) Control cells (+/+) and ARID1A-depleted (-/-) HCT116 cells were exposed to IR (10 Gy) and DNA content (A) and phosphor-Histone H3 (B) were determined at indicated time points post IR.

(C) Control cells (+/+) and ARID1A-depleted (-/-) HCT116 cells were exposed to IR (10 Gy) or left untreated and subsequently grown in the presence of paclitaxel (2 μM). Phosphor-Histone H3 was determined at the indicated time points after IR.

(D) Western blot analyses confirm the effective ARID1A depletion in HCT116 ARID1A knockout cells.

(E) U2OS cells were stably knockdown ARID1A, BRG1 or BRM with shRNAs. Phosphor-Histone H3 was determined 16 hrs after IR in the presence of paclitaxel.

(A-D) (Left) Representative images. (Right) Quantitative results represent the mean ± SD of three independent experiments (Student's *t*-test, *<0.05).

Figure 4. ARID1A is required for DSB-induced ATR activation and checkpoint signaling.

(A-C) Control cells (+/+) and ARID1A-depleted (-/-) HCT116 cells were exposed to IR and harvested at indicated time points. Whole cell lysates were immunoblotted with the indicated antibodies.

(D) Control cells (+/+) and ARID1A-depleted (-/-) HCT116 cells were exposed to IR and harvested at indicated time points. Chromatin fractionation was immunoblotted with the indicated antibodies.

(E-F) Control cells (+/+) and ARID1A-depleted (-/-) HCT116 cells were exposed to IR and immunostained with indicated antibodies. (Left) Representative images, Scale bar,

10μM. (Right) Data are presented from 3 independent experiments (Student's *t*-test, *<0.01).

Figure 5. ARID1A promotes DSB end resection.

(A and B) Western blot analysis of RPA phosphorylation (p-RPAS4/S8) at indicated time points after IR (A) or replication stress stimuli (HU 2mM and UV 50 J/m^2) (B) in Control cells (+/+) and ARID1A-depleted (-/-) HCT116 cells.

(C) Control cells (+/+) and ARID1A-depleted (-/-) HCT116 cells were exposed to IR and immunostained with p-RPAS4/S8. (Left) Representative images, Scale bar, 10μM. (Right) Data are presented from 3 independent experiments (*<0.01).

(D) DRGFP U2OS cells were transfected with control siRNA or ARID1A siRNA (SMARTpool). Fourty-eight hours later, cells were transfected with I-SceI plasmid. ChIP assay was conducted 8 hrs after I-SceI transfection and qPCR analyses were used to detect the relative enrichment of H3 to the IgG control (Average ± SEM; n=3; Student's *t*-test,* p<0.01). Western blot analyses to demonstrate the effectiveARID1A knockdown were shown next to the graph.

(E and F) Defective HR repair (E) and SSA repair (F) in ARID1A-deficient cells upon DSB induced by I-SceI. (Left) Representative flow cytometry profile. (Right) Each value is relative to the percentage of GFP+ cells in I-SceI-transfected cells without siRNA transfection, which was set to 1 and represents the mean ± SD of three independent experiments; Student's *t*-test (* p<0.01). Western blot analyses to demonstrate the effectiveARID1A knockdown were shown next to the graph.

Figure 6. ARID1A deficiency sensitizes cells to PARP inhibitors.

(A-C) ARID1A stably knockdown non-transformed normal breast epithelial cells MCF10A (A) and HMEC (B), ARID1A knockout HCT116 cells (C) were treated with indicated PARP inhibitors (Veliparib, Olaparib, Rucaparib, BMN673 concentrations, 10μM each). Clonogenic assay was performed. (Left) Representative images. (Right) Quantitative results represent the mean ± SD of three independent experiments, Student's *t*-test (* $p<0.01$). Western blot analyses to demonstrate the effectiveARID1A knockdown were shown next to the graph.

(D) Western blot analyses show the effectiveARID1A knockdown in MDA-MB-231cells.

(E and F) Stably ARID1A knockdown MDA-MB-231 cells (E) and ARID1A-knockout HCT116 cells (F) were treated with indicated PARP inhibitors for 72 hrs and apoptosis was determined by annexin V staining. Quantitative results represent the mean ± SD of three independent experiments, Student's *t*-test (* $p<0.01$). Western blot analyses to demonstrate the activation of Caspase-3 in ARID1A-knockout HCT116 cells were shown next to the graph.

(G) ARID1A-knockout HCT116 cells were reconstituted with wildtype or mutant (5548delG) ARID1A transiently and exposed to BMN673 for 48 hrs. Apoptosis was determined by annexin V staining (the mean ± SD of three independent experiments, Student's *t*-test * $p<0.01$).

(H) ARID1A-knockout HCT116 cells were exposed to Rucaparib or BMN673 in a dose-dependent manner for 48 hrs. Apoptosis was determined by annexin V staining (the mean ± SD of three independent experiments).

Figure 7. BMN673 selectively inhibits ARID1A-deficient xenograft tumor growth.

(A) Representative images of MDA-MB-231 and HCT116 xenografts treated with vehicle control and BMN673 at the end point of scheduled treatment.

(C-D) Control and ARID1A-depleted HCT116 (B and C) and MDA-MB-231 cells were inoculated subcutaneously in athymic nu/nu mice. Mice were randomized into vehicle control and BMN673 treatment group. Average tumor volum was plotted against days of treatment (n=6 for each group, Student's *t*-test * $p<0.01$).

(F) Average tumor volume of each group was determined at the end of the scheduled treatment (n=6 for each group, Student's *t*-test * $p<0.01$).

(H) Examples of the IHC analyses of xenograft tumors with anti-phospho-CHK1 (S317) and anti-actived caspase 3 antibodies. Scale bar, 50μM. Quantification of anti-phospho-CHK1 (S317) and anti-actived caspase 3-positive cells of 3 individual tumors (Student's *t*-test * $p<0.01$)

Figure S1. Proteomic analysis of ATR-interacting proteins. Proteins identified from our proteomic analysis was shown.

Figure S2. Schematic diagram of KillerRed system in U2OS TRE cells. KillerRed (KR) is a light-stimulated ROS-inducer fused to a tet-repressor (tetR-KR), which binds to a TRE cassette (~ 90 kb) integrated at a defined genomic locus in U2OS cells (U2OS TRE cell line). By targeting the expression of KR to one specific genome site, the recruitment of proteins at DNA damaged genetic loci can be visualized.

Figure S3. Knockdown BRG1, BRM or ARID1A in U2OS cells. U2OS cells were infected with shRNA vectors targeting BRG1, BRM or ARID1A. After puromycin selection, knockdown efficiency was shown by Western blot analyses with indicated antibodies.

Figure S4. ARID1A depletion did not affect the number of ATM foci formation after IR. Control cells (+/+) and ARID1A-depleted (-/-) HCT116 cells were exposed to IR and immunostained with p-ATM (S1981). (Top) Representative images, Scale bar, 10μM. (Bottom) Data are presented from 3 independent experiments (*<0.01).

Figure S5. ARID1A depletion did not affect the presence of DSBs after IR. Control cells (+/+) and ARID1A-depleted (-/-) HCT116 cells were exposed to IR and DSBs were detected by the Comet Assay. (Left) Representative images, Scale bar, 10μM. (Right) Data are presented from 3 independent experiments (n.s. Student t-test did not find statistical significance).

Figure S6. ARID1A depletion did not affect the expression of DSB end resection factors. (Left) Schematic diagrams of HR repair assay and SSA repair assay. In these two assays, DSB is induced by transfection I-SceI restriction enzyme and repaired via HR or SSA mechanism, which generate GFP positive cells. (Right) Control cells (+/+) and ARID1A-depleted (-/-) HCT116 cells were exposed to IR and Western blot analyses were performed to examine the expression levels of DSB end resection factors with indicated antibodies.

Figure S7. ARID1A depletion did not affect the expression of ATM and MRN complex. Control cells (+/+) and ARID1A-depleted (-/-) HCT116 cells were exposed to IR and Western blot analyses were performed with indicated antibodies.

Reference:

Adams, K. E., Medhurst, A. L., Dart, D. A., and Lakin, N. D. (2006). Recruitment of ATR to sites of ionising radiation-induced DNA damage requires ATM and components of the MRN protein complex. Oncogene *25*, 3894-3904.

Bennardo, N., Cheng, A., Huang, N., and Stark, J. M. (2008). Alternative-NHEJ is a mechanistically distinct pathway of mammalian chromosome break repair. PLoS Genet *4*, e1000110.

Berkovich, E., Monnat, R. J., Jr., and Kastan, M. B. (2007). Roles of ATM and NBS1 in chromatin structure modulation and DNA double-strand break repair. Nat Cell Biol *9*, 683-690.

Brown, E. J. (2003). The ATR-independent DNA replication checkpoint. Cell Cycle *2*, 188-189.

Brown, E. J., and Baltimore, D. (2000). ATR disruption leads to chromosomal fragmentation and early embryonic lethality. Genes Dev *14*, 397-402.

Bryant, H. E., Schultz, N., Thomas, H. D., Parker, K. M., Flower, D., Lopez, E., Kyle, S., Meuth, M., Curtin, N. J., and Helleday, T. (2005). Specific killing of BRCA2-deficient tumours with inhibitors of poly(ADP-ribose) polymerase. Nature *434*, 913-917.

Budd, M. E., and Campbell, J. L. (2009). Interplay of Mre11 nuclease with Dna2 plus Sgs1 in Rad51-dependent recombinational repair. PLoS One *4*, e4267.

Cardnell, R. J., Feng, Y., Diao, L., Fan, Y. H., Masrorpour, F., Wang, J., Shen, Y., Mills, G. B., Minna, J. D., Heymach, J. V., and Byers, L. A. (2013). Proteomic markers of DNA repair and PI3K pathway activation predict response to the PARP inhibitor BMN 673 in small cell lung cancer. Clin Cancer Res *19*, 6322-6328.

Carpentier, P., Violot, S., Blanchoin, L., and Bourgeois, D. (2009). Structural basis for the phototoxicity of the fluorescent protein KillerRed. FEBS Lett *583*, 2839-2842.

Chen, X., Cui, D., Papusha, A., Zhang, X., Chu, C. D., Tang, J., Chen, K., Pan, X., and Ira, G. (2012). The Fun30 nucleosome remodeller promotes resection of DNA double-strand break ends. Nature *489*, 576-580.

Ciccia, A., and Elledge, S. J. (2010). The DNA damage response: making it safe to play with knives. Mol Cell *40*, 179-204.

Cimprich, K. A., and Cortez, D. (2008). ATR: an essential regulator of genome integrity. Nat Rev Mol Cell Biol *9*, 616-627.

Clerici, M., Mantiero, D., Lucchini, G., and Longhese, M. P. (2005). The Saccharomyces cerevisiae Sae2 protein promotes resection and bridging of double strand break ends. J Biol Chem *280*, 38631-38638.
Cortez, D., Guntuku, S., Qin, J., and Elledge, S. J. (2001). ATR and ATRIP: partners in checkpoint signaling. Science *294*, 1713-1716.
Costelloe, T., Louge, R., Tomimatsu, N., Mukherjee, B., Martini, E., Khadaroo, B., Dubois, K., Wiegant, W. W., Thierry, A., Burma, S.*, et al.* (2012). The yeast Fun30 and human SMARCAD1 chromatin remodellers promote DNA end resection. Nature *489*, 581-584.
Dykhuizen, E. C., Hargreaves, D. C., Miller, E. L., Cui, K., Korshunov, A., Kool, M., Pfister, S., Cho, Y. J., Zhao, K., and Crabtree, G. R. (2013). BAF complexes facilitate decatenation of DNA by topoisomerase IIalpha. Nature *497*, 624-627.
Ellisen, L. W. (2011). PARP inhibitors in cancer therapy: promise, progress, and puzzles. Cancer Cell *19*, 165-167.
Eroglu, E., Burkard, T. R., Jiang, Y., Saini, N., Homem, C. C., Reichert, H., and Knoblich, J. A. (2014). SWI/SNF Complex Prevents Lineage Reversion and Induces Temporal Patterning in Neural Stem Cells. Cell *156*, 1259-1273.
Falck, J., Coates, J., and Jackson, S. P. (2005). Conserved modes of recruitment of ATM, ATR and DNA-PKcs to sites of DNA damage. Nature *434*, 605-611.
Farmer, H., McCabe, N., Lord, C. J., Tutt, A. N., Johnson, D. A., Richardson, T. B., Santarosa, M., Dillon, K. J., Hickson, I., Knights, C.*, et al.* (2005). Targeting the DNA repair defect in BRCA mutant cells as a therapeutic strategy. Nature *434*, 917-921.
Gravel, S., Chapman, J. R., Magill, C., and Jackson, S. P. (2008). DNA helicases Sgs1 and BLM promote DNA double-strand break resection. Genes Dev *22*, 2767-2772.
Guan, B., Wang, T. L., and Shih Ie, M. (2011). ARID1A, a factor that promotes formation of SWI/SNF-mediated chromatin remodeling, is a tumor suppressor in gynecologic cancers. Cancer Res *71*, 6718-6727.
Harper, J. W., and Elledge, S. J. (2007). The DNA damage response: ten years after. Mol Cell *28*, 739-745.
Helming, K. C., Wang, X., Wilson, B. G., Vazquez, F., Haswell, J. R., Manchester, H. E., Kim, Y., Kryukov, G. V., Ghandi, M., Aguirre, A. J.*, et al.* (2014). ARID1B is a specific vulnerability in ARID1A-mutant cancers. Nat Med *20*, 251-254.
Imbalzano, A. N., Kwon, H., Green, M. R., and Kingston, R. E. (1994). Facilitated binding of TATA-binding protein to nucleosomal DNA. Nature *370*, 481-485.
Jackson, S. P., and Bartek, J. (2009). The DNA-damage response in human biology and disease. Nature *461*, 1071-1078.
Jazayeri, A., Falck, J., Lukas, C., Bartek, J., Smith, G. C., Lukas, J., and Jackson, S. P. (2006). ATM- and cell cycle-dependent regulation of ATR in response to DNA double-strand breaks. Nat Cell Biol *8*, 37-45.
Jones, S., Li, M., Parsons, D. W., Zhang, X., Wesseling, J., Kristel, P., Schmidt, M. K., Markowitz, S., Yan, H., Bigner, D.*, et al.* (2012). Somatic mutations in the chromatin remodeling gene ARID1A occur in several tumor types. Hum Mutat *33*, 100-103.
Kozlov, S. V., Graham, M. E., Peng, C., Chen, P., Robinson, P. J., and Lavin, M. F. (2006). Involvement of novel autophosphorylation sites in ATM activation. EMBO J *25*, 3504-3514.

Kwon, H., Imbalzano, A. N., Khavari, P. A., Kingston, R. E., and Green, M. R. (1994). Nucleosome disruption and enhancement of activator binding by a human SW1/SNF complex. Nature *370*, 477-481.
Lan, L., Ui, A., Nakajima, S., Hatakeyama, K., Hoshi, M., Watanabe, R., Janicki, S. M., Ogiwara, H., Kohno, T., Kanno, S., and Yasui, A. (2010). The ACF1 complex is required for DNA double-strand break repair in human cells. Mol Cell *40*, 976-987.
Lee, J. H., and Paull, T. T. (2005). ATM activation by DNA double-strand breaks through the Mre11-Rad50-Nbs1 complex. Science *308*, 551-554.
Li, X. S., Trojer, P., Matsumura, T., Treisman, J. E., and Tanese, N. (2010). Mammalian SWI/SNF--a subunit BAF250/ARID1 is an E3 ubiquitin ligase that targets histone H2B. Mol Cell Biol *30*, 1673-1688.
Limbo, O., Chahwan, C., Yamada, Y., de Bruin, R. A., Wittenberg, C., and Russell, P. (2007). Ctp1 is a cell-cycle-regulated protein that functions with Mre11 complex to control double-strand break repair by homologous recombination. Mol Cell *28*, 134-146.
Liu, S., Shiotani, B., Lahiri, M., Marechal, A., Tse, A., Leung, C. C., Glover, J. N., Yang, X. H., and Zou, L. (2011). ATR autophosphorylation as a molecular switch for checkpoint activation. Mol Cell *43*, 192-202.
Matsuoka, S., Ballif, B. A., Smogorzewska, A., McDonald, E. R., 3rd, Hurov, K. E., Luo, J., Bakalarski, C. E., Zhao, Z., Solimini, N., Lerenthal, Y.*, et al.* (2007). ATM and ATR substrate analysis reveals extensive protein networks responsive to DNA damage. Science *316*, 1160-1166.
Mimitou, E. P., and Symington, L. S. (2008). Sae2, Exo1 and Sgs1 collaborate in DNA double-strand break processing. Nature *455*, 770-774.
Myers, J. S., and Cortez, D. (2006). Rapid activation of ATR by ionizing radiation requires ATM and Mre11. J Biol Chem *281*, 9346-9350.
Nagl, N. G., Jr., Patsialou, A., Haines, D. S., Dallas, P. B., Beck, G. R., Jr., and Moran, E. (2005). The p270 (ARID1A/SMARCF1) subunit of mammalian SWI/SNF-related complexes is essential for normal cell cycle arrest. Cancer Res *65*, 9236-9244.
Nam, E. A., Zhao, R., Glick, G. G., Bansbach, C. E., Friedman, D. B., and Cortez, D. (2011). Thr-1989 phosphorylation is a marker of active ataxia telangiectasia-mutated and Rad3-related (ATR) kinase. J Biol Chem *286*, 28707-28714.
Nimonkar, A. V., Genschel, J., Kinoshita, E., Polaczek, P., Campbell, J. L., Wyman, C., Modrich, P., and Kowalczykowski, S. C. (2011). BLM-DNA2-RPA-MRN and EXO1-BLM-RPA-MRN constitute two DNA end resection machineries for human DNA break repair. Genes Dev *25*, 350-362.
Panier, S., and Boulton, S. J. (2014). Double-strand break repair: 53BP1 comes into focus. Nat Rev Mol Cell Biol *15*, 7-18.
Peng, G., Yim, E. K., Dai, H., Jackson, A. P., Burgt, I., Pan, M. R., Hu, R., Li, K., and Lin, S. Y. (2009). BRIT1/MCPH1 links chromatin remodelling to DNA damage response. Nat Cell Biol *11*, 865-872.
Phelan, M. L., Sif, S., Narlikar, G. J., and Kingston, R. E. (1999). Reconstitution of a core chromatin remodeling complex from SWI/SNF subunits. Mol Cell *3*, 247-253.
Pierce, A. J., Johnson, R. D., Thompson, L. H., and Jasin, M. (1999). XRCC3 promotes homology-directed repair of DNA damage in mammalian cells. Genes Dev *13*, 2633-2638.

Pletnev, S., Gurskaya, N. G., Pletneva, N. V., Lukyanov, K. A., Chudakov, D. M., Martynov, V. I., Popov, V. O., Kovalchuk, M. V., Wlodawer, A., Dauter, Z., and Pletnev, V. (2009). Structural basis for phototoxicity of the genetically encoded photosensitizer KillerRed. J Biol Chem *284*, 32028-32039.
Polo, S. E., Blackford, A. N., Chapman, J. R., Baskcomb, L., Gravel, S., Rusch, A., Thomas, A., Blundred, R., Smith, P., Kzhyshkowska, J.*, et al.* (2012). Regulation of DNA-end resection by hnRNPU-like proteins promotes DNA double-strand break signaling and repair. Mol Cell *45*, 505-516.
Roberts, C. W., and Biegel, J. A. (2009). The role of SMARCB1/INI1 in development of rhabdoid tumor. Cancer Biol Ther *8*, 412-416.
Roberts, C. W., and Orkin, S. H. (2004). The SWI/SNF complex--chromatin and cancer. Nat Rev Cancer *4*, 133-142.
Sartori, A. A., Lukas, C., Coates, J., Mistrik, M., Fu, S., Bartek, J., Baer, R., Lukas, J., and Jackson, S. P. (2007). Human CtIP promotes DNA end resection. Nature *450*, 509-514.
Schlacher, K., Christ, N., Siaud, N., Egashira, A., Wu, H., and Jasin, M. (2011). Double-strand break repair-independent role for BRCA2 in blocking stalled replication fork degradation by MRE11. Cell *145*, 529-542.
Shen, Y., Rehman, F. L., Feng, Y., Boshuizen, J., Bajrami, I., Elliott, R., Wang, B., Lord, C. J., Post, L. E., and Ashworth, A. (2013). BMN 673, a novel and highly potent PARP1/2 inhibitor for the treatment of human cancers with DNA repair deficiency. Clin Cancer Res *19*, 5003-5015.
Varela, I., Tarpey, P., Raine, K., Huang, D., Ong, C. K., Stephens, P., Davies, H., Jones, D., Lin, M. L., Teague, J.*, et al.* (2011). Exome sequencing identifies frequent mutation of the SWI/SNF complex gene PBRM1 in renal carcinoma. Nature *469*, 539-542.
Vogelstein, B., Papadopoulos, N., Velculescu, V. E., Zhou, S., Diaz, L. A., Jr., and Kinzler, K. W. (2013). Cancer genome landscapes. Science *339*, 1546-1558.
Wang, G. G., Allis, C. D., and Chi, P. (2007). Chromatin remodeling and cancer, Part II: ATP-dependent chromatin remodeling. Trends Mol Med *13*, 373-380.
Wang, X., Nagl, N. G., Jr., Flowers, S., Zweitzig, D., Dallas, P. B., and Moran, E. (2004a). Expression of p270 (ARID1A), a component of human SWI/SNF complexes, in human tumors. Int J Cancer *112*, 636.
Wang, X., Nagl, N. G., Wilsker, D., Van Scoy, M., Pacchione, S., Yaciuk, P., Dallas, P. B., and Moran, E. (2004b). Two related ARID family proteins are alternative subunits of human SWI/SNF complexes. Biochem J *383*, 319-325.
Wilson, B. G., and Roberts, C. W. (2011). SWI/SNF nucleosome remodellers and cancer. Nat Rev Cancer *11*, 481-492.
Wu, J. N., and Roberts, C. W. (2013). ARID1A Mutations in Cancer: Another Epigenetic Tumor Suppressor? Cancer Discov *3*, 35-43.
Wu, R. C., Wang, T. L., and Shih, I. M. (2014). The emerging roles of ARID1A in tumor suppression. Cancer Biol Ther *15*.
Zhou, B. B., and Elledge, S. J. (2000). The DNA damage response: putting checkpoints in perspective. Nature *408*, 433-439.
Zou, L., and Elledge, S. J. (2003). Sensing DNA damage through ATRIP recognition of RPA-ssDNA complexes. Science *300*, 1542-1548.

Figure 1

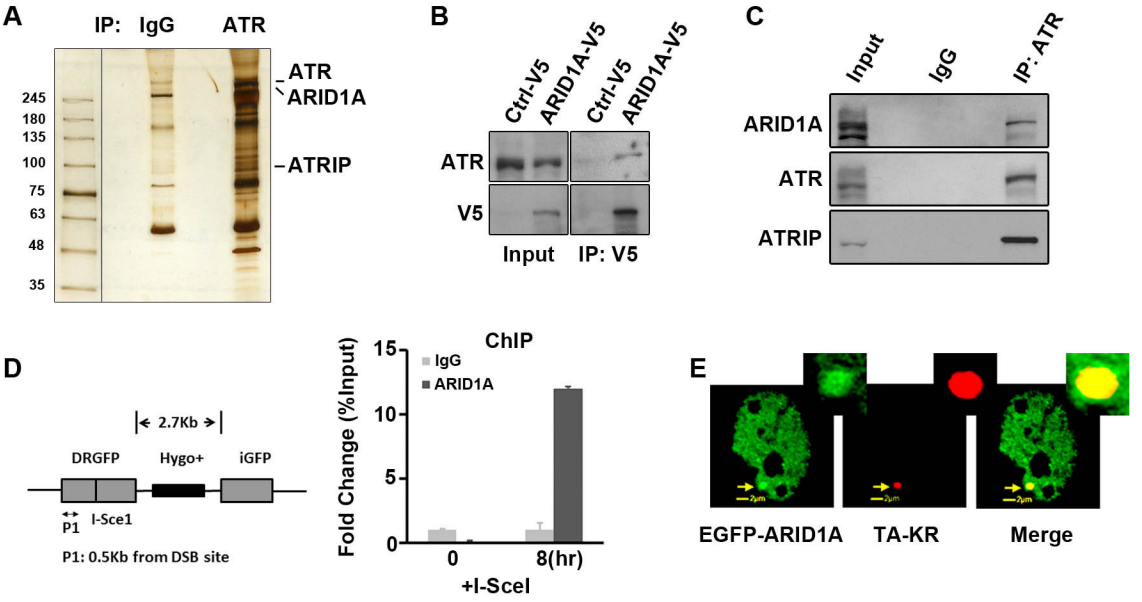
A
IP: IgG ATR
245
180
135
100
75
63
48
35
ATR
ARID1A
ATRIP
B
Ctrl-V5
ARID1A-V5
Ctrl-V5
ARID1A-V5
ATR
V5
Input
IP: V5
C
Input
IgG
IP: ATR
ARID1A
ATR
ATRIP
D
2.7Kb
DRGFP
Hygo+
iGFP
P1
I-Sce1
P1: 0.5Kb from DSB site
ChIP
IgG
ARID1A
Fold Change (%Input)
15
10
5
0
0
8(hr)
+I-SceI
E
EGFP-ARID1A
TA-KR
Merge

Figure 2

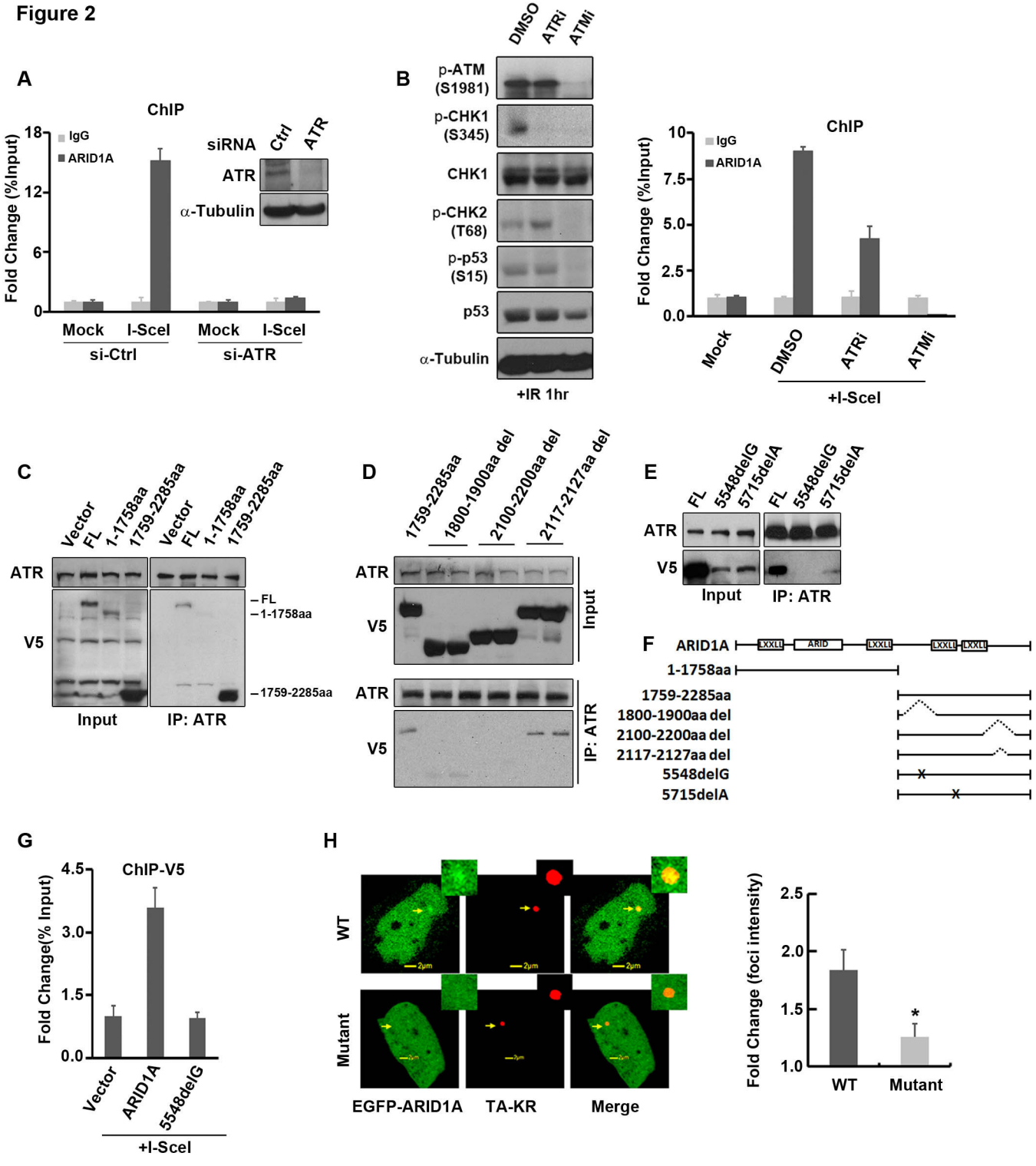
A
ChIP
IgG
ARID1A
Fold Change (%Input)
siRNA
Ctrl
ATR
ATR
α-Tubulin
Mock
I-SceI
Mock
I-SceI
si-Ctrl
si-ATR
B
DMSO
ATRi
ATMi
p-ATM (S1981)
p-CHK1 (S345)
CHK1
p-CHK2 (T68)
p-p53 (S15)
p53
α-Tubulin
+IR 1hr
ChIP
IgG
ARID1A
Fold Change (%Input)
Mock
DMSO
ATRi
ATMi
+I-SceI
C
Vector
FL
1-1758aa
1759-2285aa
Vector
FL
1-1758aa
1759-2285aa
ATR
V5
FL
1-1758aa
1759-2285aa
Input
IP: ATR
D
1759-2285aa
1800-1900aa del
2100-2200aa del
2117-2127aa del
ATR
V5
Input
ATR
V5
IP: ATR
E
FL
5548delG
5715delA
FL
5548delG
5715delA
ATR
V5
Input
IP: ATR
F
ARID1A
LXXLL
ARID
LXXLL
LXXLL
LXXLL
1-1758aa
1759-2285aa
1800-1900aa del
2100-2200aa del
2117-2127aa del
5548delG
5715delA
G
ChIP-V5
Fold Change(% Input)
Vector
ARID1A
5548delG
+I-SceI
H
WT
Mutant
EGFP-ARID1A
TA-KR
Merge
Fold Change (foci intensity)
WT
Mutant

Figure 3

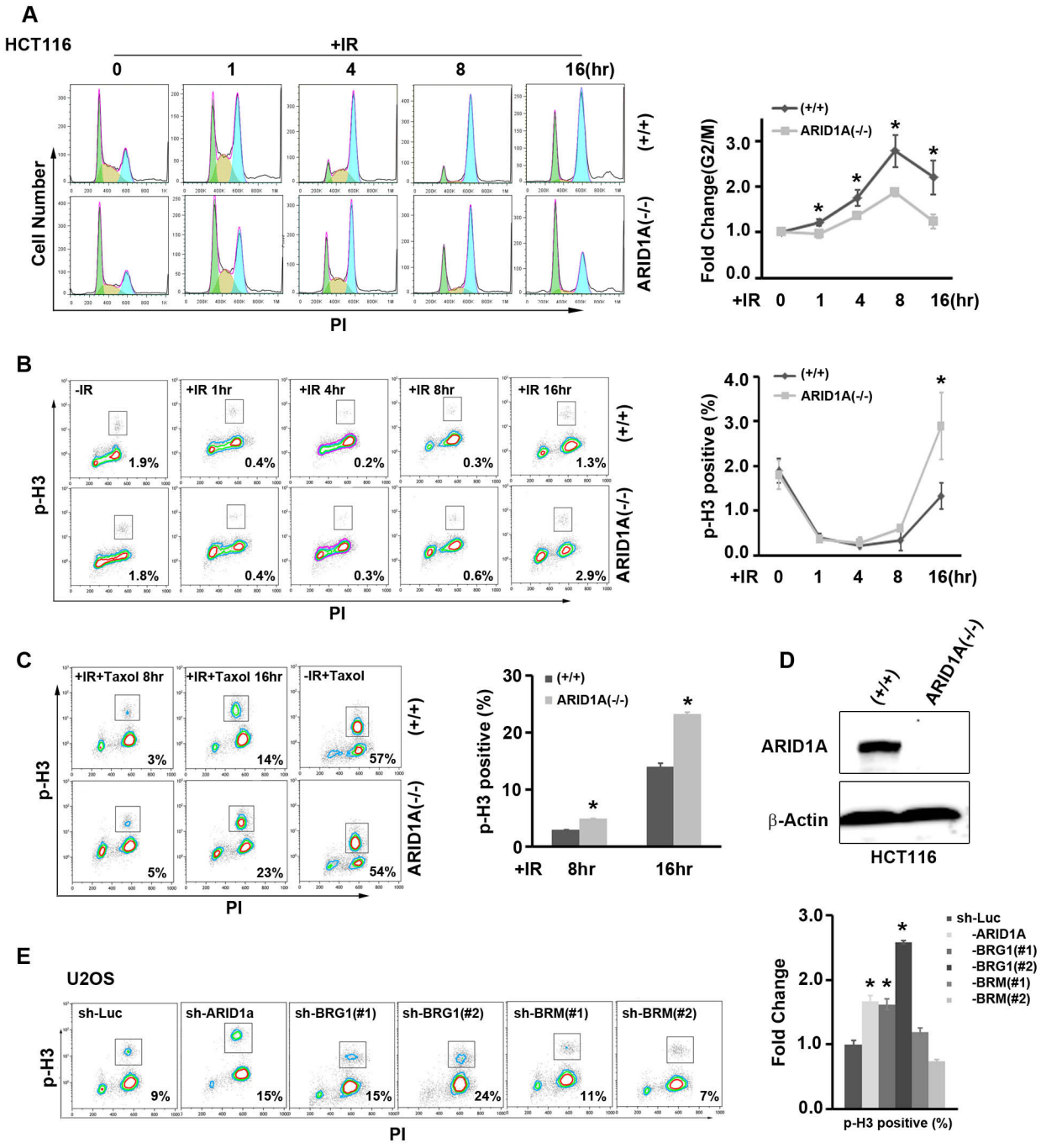
A
HCT116
+IR
0
1
4
8
16(hr)
Cell Number
PI
(+/+)
ARID1A(-/-)
Fold Change(G2/M)
+IR 0 1 4 8 16(hr)
B
-IR
+IR 1hr
+IR 4hr
+IR 8hr
+IR 16hr
p-H3
1.9%
0.4%
0.2%
0.3%
1.3%
1.8%
0.4%
0.3%
0.6%
2.9%
p-H3 positive (%)
C
+IR+Taxol 8hr
+IR+Taxol 16hr
-IR+Taxol
3%
14%
57%
5%
23%
54%
+IR 8hr 16hr
D
ARID1A
β-Actin
HCT116
E
U2OS
sh-Luc
sh-ARID1a
sh-BRG1(#1)
sh-BRG1(#2)
sh-BRM(#1)
sh-BRM(#2)
9%
15%
15%
24%
11%
7%
-ARID1A
-BRG1(#1)
-BRG1(#2)
-BRM(#1)
-BRM(#2)
Fold Change
p-H3 positive (%)

Figure 4

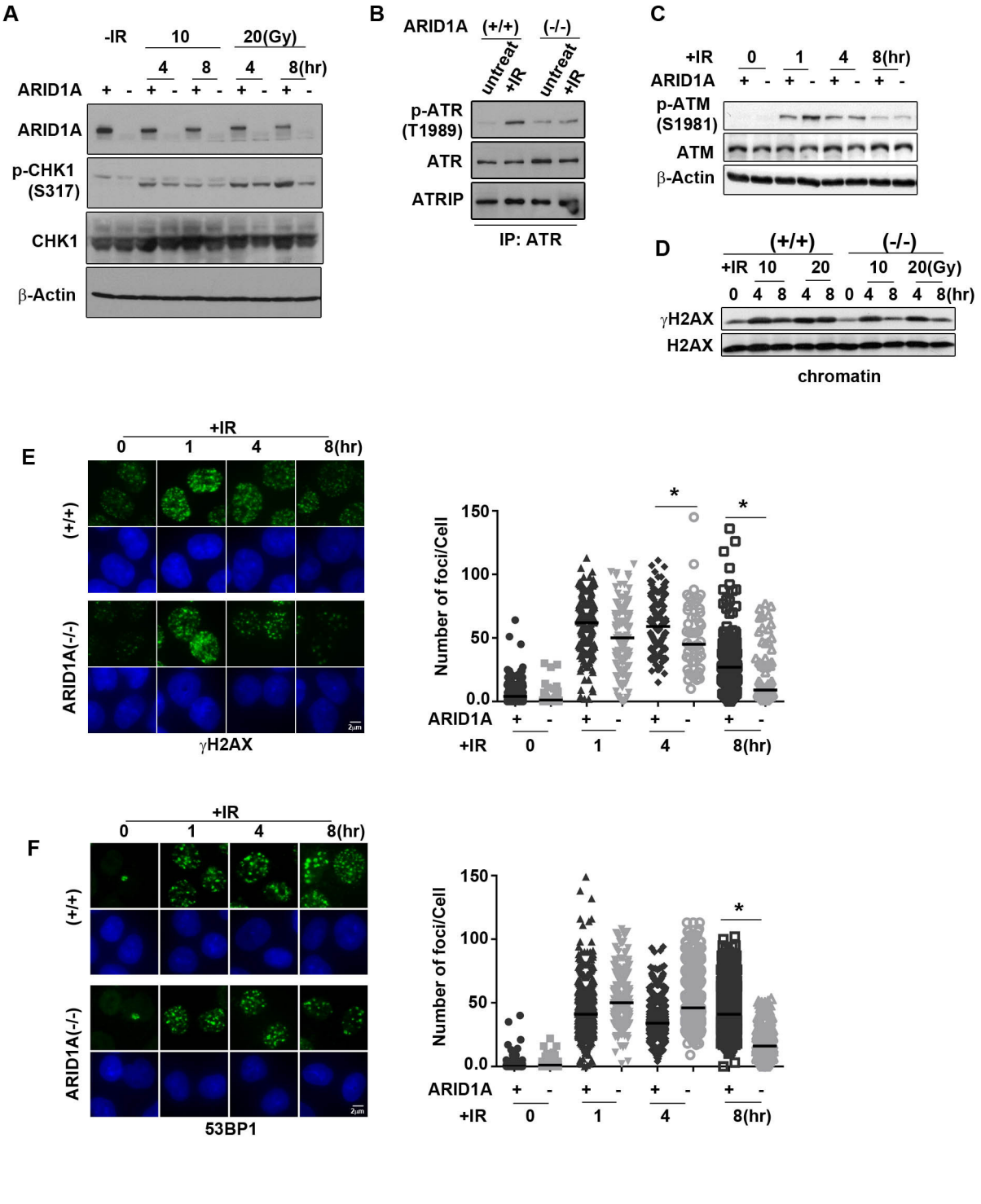
A
-IR
10
20(Gy)
4
8
4
8(hr)
ARID1A + - + - + - + - + -
ARID1A
p-CHK1 (S317)
CHK1
β-Actin
B
ARID1A (+/+) (-/-)
untreat
+IR
untreat
+IR
p-ATR (T1989)
ATR
ATRIP
IP: ATR
C
+IR 0 1 4 8(hr)
ARID1A + - + - + - + -
p-ATM (S1981)
ATM
β-Actin
D
(+/+)
(-/-)
+IR 10 20 10 20(Gy)
0 4 8 4 8 0 4 8 4 8(hr)
γH2AX
H2AX
chromatin
E
+IR
0 1 4 8(hr)
(+/+)
ARID1A(-/-)
γH2AX
Number of foci/Cell
150
100
50
0.0
*
*
ARID1A + - + - + - + -
+IR 0 1 4 8(hr)
F
+IR
0 1 4 8(hr)
(+/+)
ARID1A(-/-)
53BP1
Number of foci/Cell
150
100
50
0.0
*
ARID1A + - + - + - + -
+IR 0 1 4 8(hr)

Figure 5

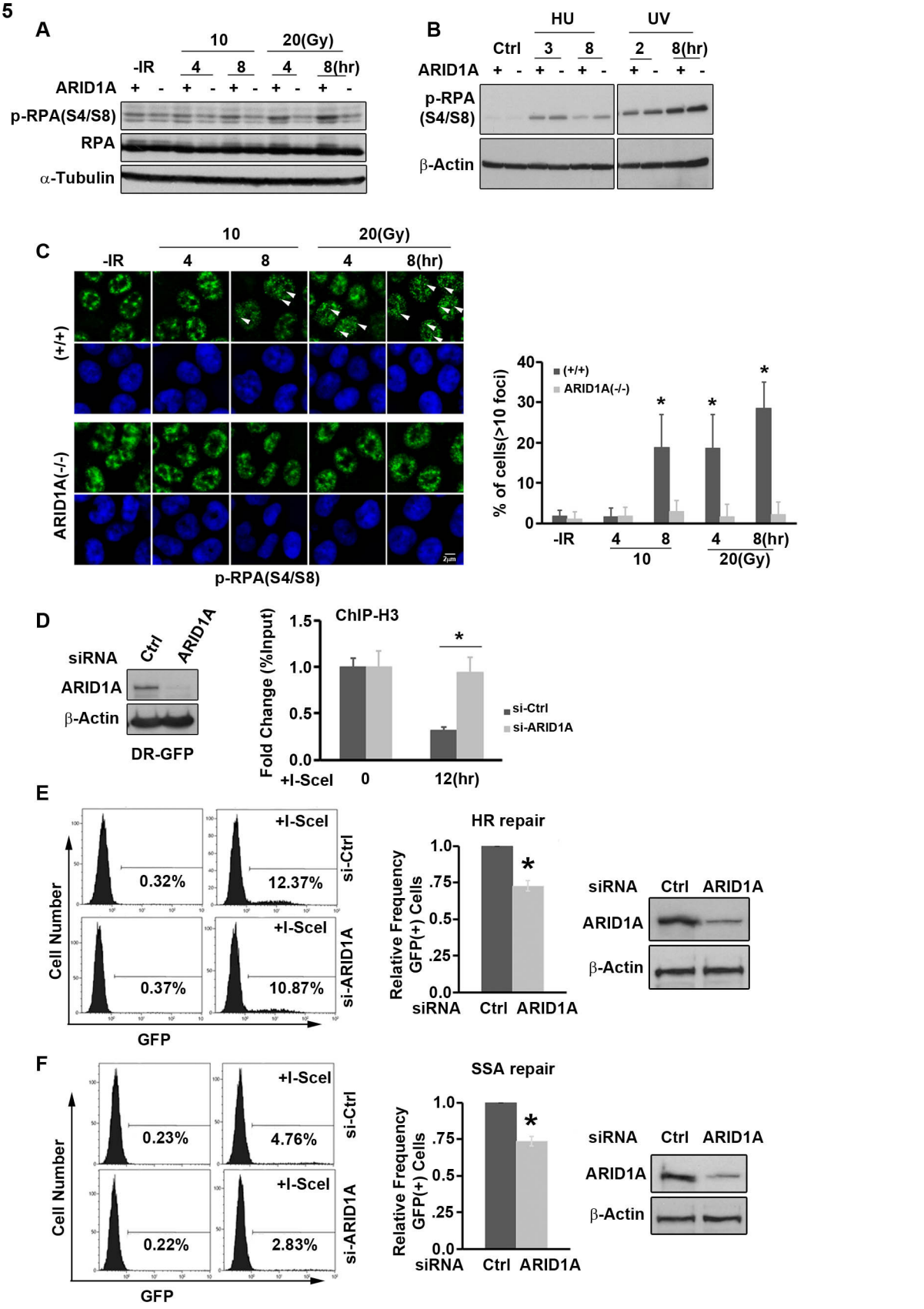
A
10
20(Gy)
-IR
4
8
4
8(hr)
ARID1A + - + - + - + - + -
p-RPA(S4/S8)
RPA
α-Tubulin
B
HU
UV
Ctrl
3
8
2
8(hr)
ARID1A + - + - + - + - + -
p-RPA (S4/S8)
β-Actin
C
10
20(Gy)
-IR
4
8
4
8(hr)
(+/+)
ARID1A(-/-)
p-RPA(S4/S8)
(+/+)
ARID1A(-/-)
% of cells(>10 foci)
40
30
20
10
0
-IR
4
8
4
8(hr)
10
20(Gy)
D
siRNA
Ctrl
ARID1A
ARID1A
β-Actin
DR-GFP
ChIP-H3
Fold Change (%Input)
1.5
1.0
0.5
0.0
+I-SceI
0
12(hr)
si-Ctrl
si-ARID1A
E
+I-SceI
0.32%
12.37%
si-Ctrl
+I-SceI
0.37%
10.87%
si-ARID1A
Cell Number
GFP
HR repair
Relative Frequency GFP(+) Cells
1.0
.75
0.5
.25
0.0
siRNA
Ctrl
ARID1A
siRNA
Ctrl
ARID1A
ARID1A
β-Actin
F
+I-SceI
0.23%
4.76%
si-Ctrl
+I-SceI
0.22%
2.83%
si-ARID1A
Cell Number
GFP
SSA repair
Relative Frequency GFP(+) Cells
1.0
.75
0.5
.25
0.0
siRNA
Ctrl
ARID1A
siRNA
Ctrl
ARID1A
ARID1A
β-Actin

Figure 6

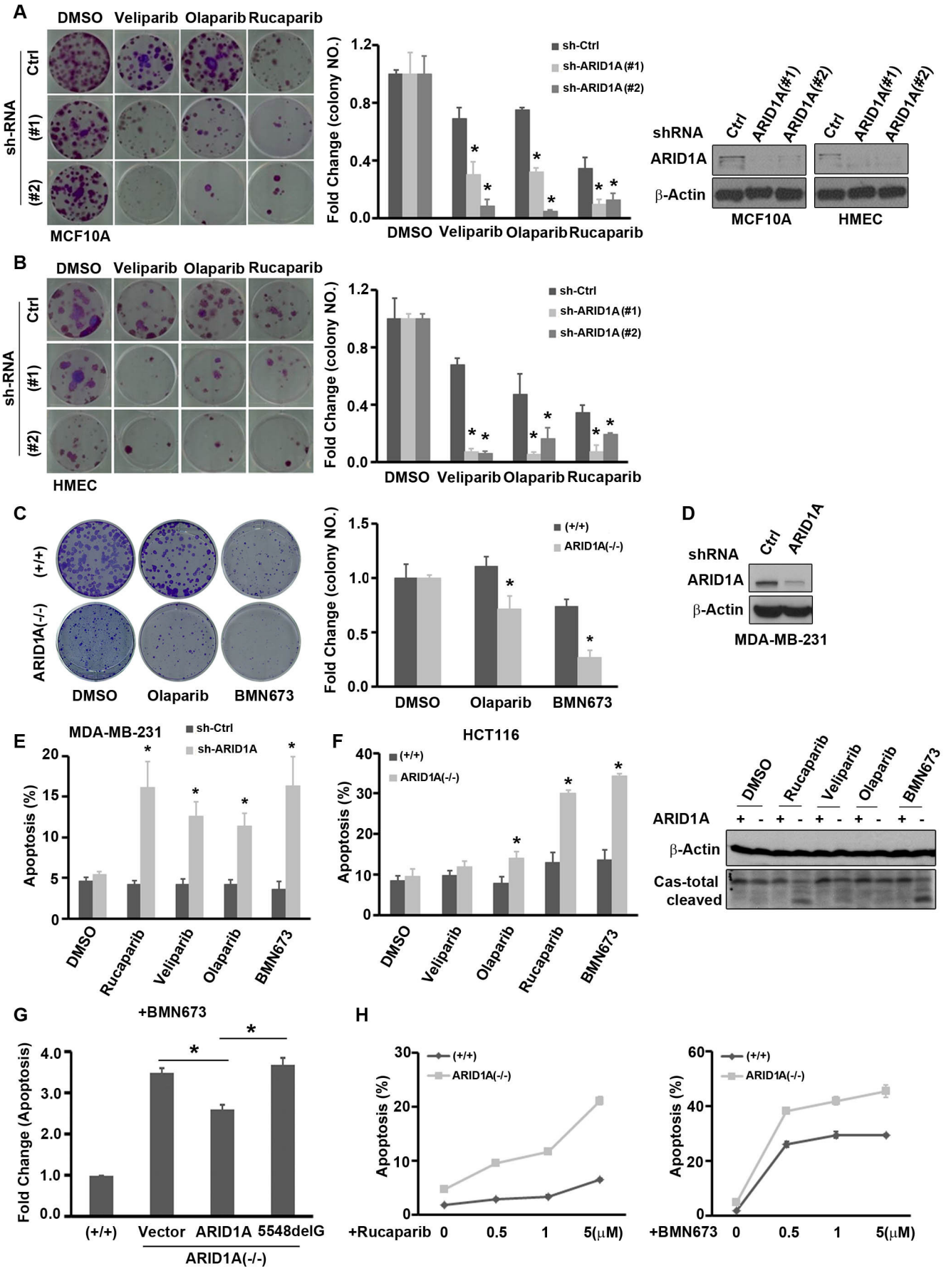
A
DMSO Veliparib Olaparib Rucaparib
sh-RNA
Ctrl
(#1)
(#2)
MCF10A
Fold Change (colony NO.)
sh-Ctrl
sh-ARID1A (#1)
sh-ARID1A (#2)
DMSO Veliparib Olaparib Rucaparib
shRNA
Ctrl
ARID1A(#1)
ARID1A(#2)
ARID1A
β-Actin
MCF10A
HMEC
B
HMEC
C
(+/+)
ARID1A(-/-)
DMSO
Olaparib
BMN673
D
MDA-MB-231
E
MDA-MB-231
Apoptosis (%)
F
HCT116
Rucaparib
Veliparib
Cas-total
cleaved
G
+BMN673
Fold Change (Apoptosis)
(+/+)
Vector
ARID1A
5548delG
ARID1A(-/-)
H
+Rucaparib 0 0.5 1 5(μM)
+BMN673 0 0.5 1 5(μM)

Figure 7

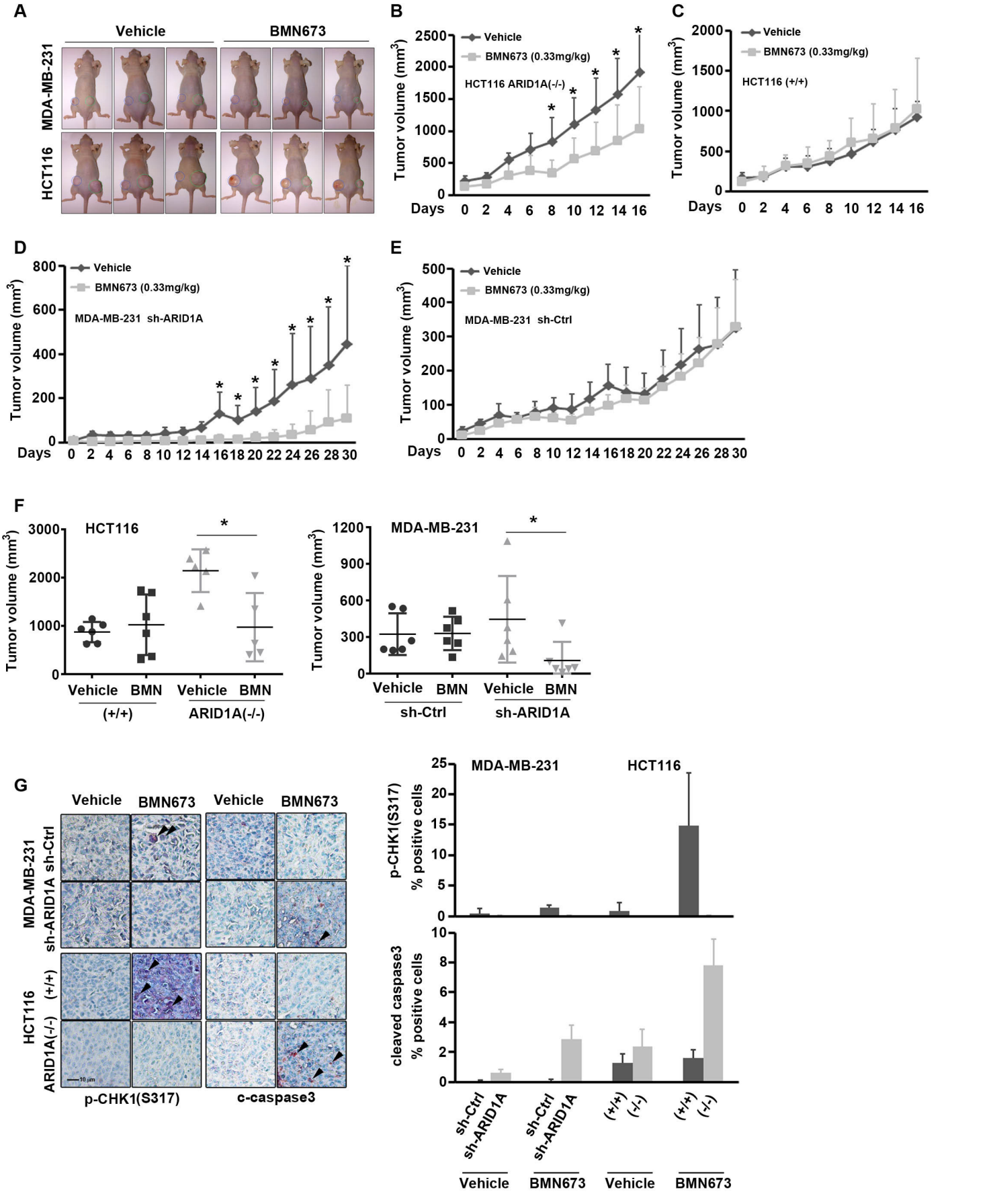
A
Vehicle
BMN673
MDA-MB-231
HCT116
B
Vehicle
BMN673 (0.33mg/kg)
HCT116 ARID1A(-/-)
Tumor volume (mm3)
Days
C
Vehicle
BMN673 (0.33mg/kg)
HCT116 (+/+)
Tumor volume (mm3)
Days
D
Vehicle
BMN673 (0.33mg/kg)
MDA-MB-231 sh-ARID1A
Tumor volume (mm3)
Days
E
Vehicle
BMN673 (0.33mg/kg)
MDA-MB-231 sh-Ctrl
Tumor volume (mm3)
Days
F
HCT116
Tumor volume (mm3)
Vehicle
BMN
Vehicle
BMN
(+/+)
ARID1A(-/-)
MDA-MB-231
Tumor volume (mm3)
Vehicle
BMN
Vehicle
BMN
sh-Ctrl
sh-ARID1A
G
Vehicle
BMN673
Vehicle
BMN673
MDA-MB-231 sh-Ctrl
sh-ARID1A
HCT116 (+/+)
ARID1A(-/-)
p-CHK1(S317)
c-caspase3
MDA-MB-231
HCT116
p-CHK1(S317) % positive cells
cleaved caspase3 % positive cells
sh-Ctrl
sh-ARID1A
sh-Ctrl
sh-ARID1A
(+/+)
(-/-)
(+/+)
(-/-)
Vehicle
BMN673
Vehicle
BMN673

ACTB_HUMAN	Actin, cytoplasmic 1 OS=Homo sapiens GN=ACTB
ACTN1_HUMAN	Alpha-actinin-1 OS=Homo sapiens GN=ACTN1
ACTN4_HUMAN	Alpha-actinin-4 OS=Homo sapiens GN=ACTN4
ADDA_HUMAN	Alpha-adducin OS=Homo sapiens GN=ADD1
ADDG_HUMAN	Gamma-adducin OS=Homo sapiens GN=ADD3
ALBU_HUMAN	Serum albumin OS=Homo sapiens GN=ALB
ATR_HUMAN	Serine/threonine-protein kinase ATR OS=Homo sapiens GN=ATR
ATRIP_HUMAN	ATR-interacting protein OS=Homo sapiens GN=ATRIP
ARI1A_HUMAN	AT-rich interactive domain-containing protein 1A OS=Homo sapiens GN=ARID1A
CAPR1_HUMAN	Caprin-1 OS=Homo sapiens GN=CAPRIN1
CLH1_HUMAN	Clathrin heavy chain 1 OS=Homo sapiens GN=CLTC
CYTSA_HUMAN	Cytospin-A OS=Homo sapiens GN=SPECC1L
DDX3X_HUMAN	ATP-dependent RNA helicase DDX3X OS=Homo sapiens GN=DDX3X
DDX5_HUMAN	Probable ATP-dependent RNA helicase DDX5 OS=Homo sapiens GN=DDX5
DHB4_HUMAN	Peroxisomal multifunctional enzyme type 2 OS=Homo sapiens GN=HSD17B4
DHX9_HUMAN	ATP-dependent RNA helicase A OS=Homo sapiens GN=DHX9
DREB_HUMAN	Drebrin OS=Homo sapiens GN=DBN1
DSG2_HUMAN	Desmoglein-2 OS=Homo sapiens GN=DSG2
ECHA_HUMAN	Trifunctional enzyme subunit alpha, mitochondrial OS=Homo sapiens GN=HADHA
EF2_HUMAN	Elongation factor 2 OS=Homo sapiens GN=EEF2
EZRI_HUMAN	Ezrin OS=Homo sapiens GN=EZR
FILA2_HUMAN	Filaggrin-2 OS=Homo sapiens GN=FLG2
FLII_HUMAN	Protein flightless-1 homolog OS=Homo sapiens GN=FLII
FLNA_HUMAN	Filamin-A OS=Homo sapiens GN=FLNA
G3BP1_HUMAN	Ras GTPase-activating protein-binding protein 1 OS=Homo sapiens GN=G3BP1
GRP75_HUMAN	Stress-70 protein, mitochondrial OS=Homo sapiens GN=HSPA9
GRP78_HUMAN	78 kDa glucose-regulated protein OS=Homo sapiens GN=HSPA5
HNRPM_HUMAN	Heterogeneous nuclear ribonucleoprotein M OS=Homo sapiens GN=HNRNPM
HNRPQ_HUMAN	Heterogeneous nuclear ribonucleoprotein Q OS=Homo sapiens GN=SYNCRIP

HNRPU_HUMAN	Heterogeneous nuclear ribonucleoprotein U OS=Homo sapiens GN=HNRNPU
HS90A_HUMAN	Heat shock protein HSP 90-alpha OS=Homo sapiens GN=HSP90AA1
HS90B_HUMAN	Heat shock protein HSP 90-beta OS=Homo sapiens GN=HSP90AB1
HSP71_HUMAN	Heat shock 70 kDa protein 1A/1B OS=Homo sapiens GN=HSPA1A
HSP7C_HUMAN	Heat shock cognate 71 kDa protein OS=Homo sapiens GN=HSPA8
IF2B2_HUMAN	Insulin-like growth factor 2 mRNA-binding protein 2 OS=Homo sapiens GN=IGF2BP2
ILF3_HUMAN	Interleukin enhancer-binding factor 3 OS=Homo sapiens GN=ILF3
K1C10_HUMAN	Keratin, type I cytoskeletal 10 OS=Homo sapiens GN=KRT10
K1C14_HUMAN	Keratin, type I cytoskeletal 14 OS=Homo sapiens GN=KRT14
K1C9_HUMAN	Keratin, type I cytoskeletal 9 OS=Homo sapiens GN=KRT9
K22E_HUMAN	Keratin, type II cytoskeletal 2 epidermal OS=Homo sapiens GN=KRT2
K2C1_HUMAN	Keratin, type II cytoskeletal 1 OS=Homo sapiens GN=KRT1
K2C5_HUMAN	Keratin, type II cytoskeletal 5 OS=Homo sapiens GN=KRT5
K2C6B_HUMAN	Keratin, type II cytoskeletal 6B OS=Homo sapiens GN=KRT6B
KCTD3_HUMAN	BTB/POZ domain-containing protein KCTD3 OS=Homo sapiens GN=KCTD3
LAP2A_HUMAN	Lamina-associated polypeptide 2, isoform alpha OS=Homo sapiens GN=TMPO
LMNA_HUMAN	Prelamin-A/C OS=Homo sapiens GN=LMNA
MPRIP_HUMAN	Myosin phosphatase Rho-interacting protein OS=Homo sapiens GN=MPRIP
MYH10_HUMAN	Myosin-10 OS=Homo sapiens GN=MYH10
MYH14_HUMAN	Myosin-14 OS=Homo sapiens GN=MYH14
MYH9_HUMAN	Myosin-9 OS=Homo sapiens GN=MYH9
MYO1B_HUMAN	Unconventional myosin-Ib OS=Homo sapiens GN=MYO1B
MYO1C_HUMAN	Unconventional myosin-Ic OS=Homo sapiens GN=MYO1C
MYO6_HUMAN	Unconventional myosin-VI OS=Homo sapiens GN=MYO6
MYPT1_HUMAN	Protein phosphatase 1 regulatory subunit 12A OS=Homo sapiens GN=PPP1R12A
NUCL_HUMAN	Nucleolin OS=Homo sapiens GN=NCL
PARP1_HUMAN	Poly [ADP-ribose] polymerase 1 OS=Homo sapiens GN=PARP1
PLAK_HUMAN	Junction plakoglobin OS=Homo sapiens GN=JUP
RAI14_HUMAN	Ankycorbin OS=Homo sapiens GN=RAI14

RS27A_HUMAN	Ubiquitin-40S ribosomal protein S27a OS=Homo sapiens GN=RPS27A
SFPQ_HUMAN	Splicing factor, proline- and glutamine-rich OS=Homo sapiens GN=SFPQ
SHKB1_HUMAN	SH3KBP1-binding protein 1 OS=Homo sapiens GN=SHKBP1
SHRM3_HUMAN	Protein Shroom3 OS=Homo sapiens GN=SHROOM3
SMTN_HUMAN	Smoothelin OS=Homo sapiens GN=SMTN
SRC8_HUMAN	Src substrate cortactin OS=Homo sapiens GN=CTTN
SUMO1_HUMAN	Small ubiquitin-related modifier 1 OS=Homo sapiens GN=SUMO1
TIF1B_HUMAN	Transcription intermediary factor 1-beta OS=Homo sapiens GN=TRIM28
TOP1_HUMAN	DNA topoisomerase 1 OS=Homo sapiens GN=TOP1
XRCC5_HUMAN	X-ray repair cross-complementing protein 5 OS=Homo sapiens GN=XRCC5
XRCC6_HUMAN	X-ray repair cross-complementing protein 6 OS=Homo sapiens GN=XRCC6

Figure S2

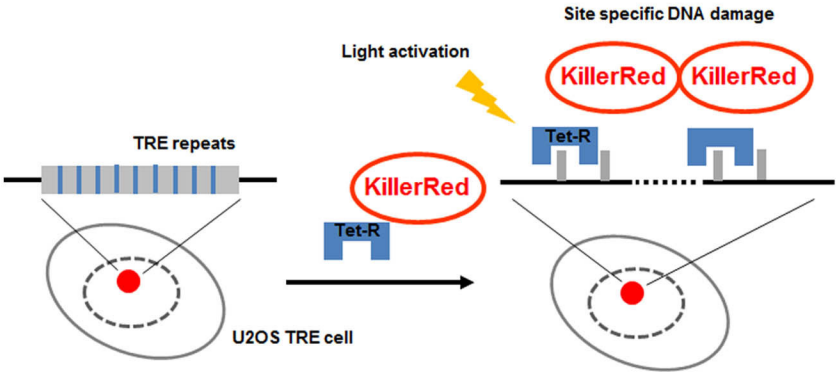
Site specific DNA damage
Light activation
KillerRed
KillerRed
Tet-R
TRE repeats
KillerRed
Tet-R
U2OS TRE cell

Figure S3

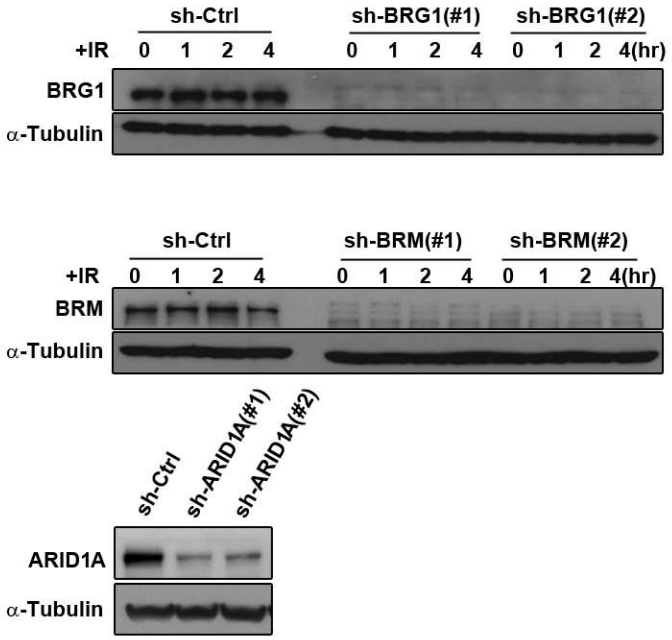
sh-Ctrl
sh-BRG1(#1)
sh-BRG1(#2)
+IR
0 1 2 4
0 1 2 4
0 1 2 4(hr)
BRG1
α-Tubulin
sh-Ctrl
sh-BRM(#1)
sh-BRM(#2)
+IR
0 1 2 4
0 1 2 4
0 1 2 4(hr)
BRM
α-Tubulin
sh-Ctrl
sh-ARID1A(#1)
sh-ARID1A(#2)
ARID1A
α-Tubulin

Figure S4

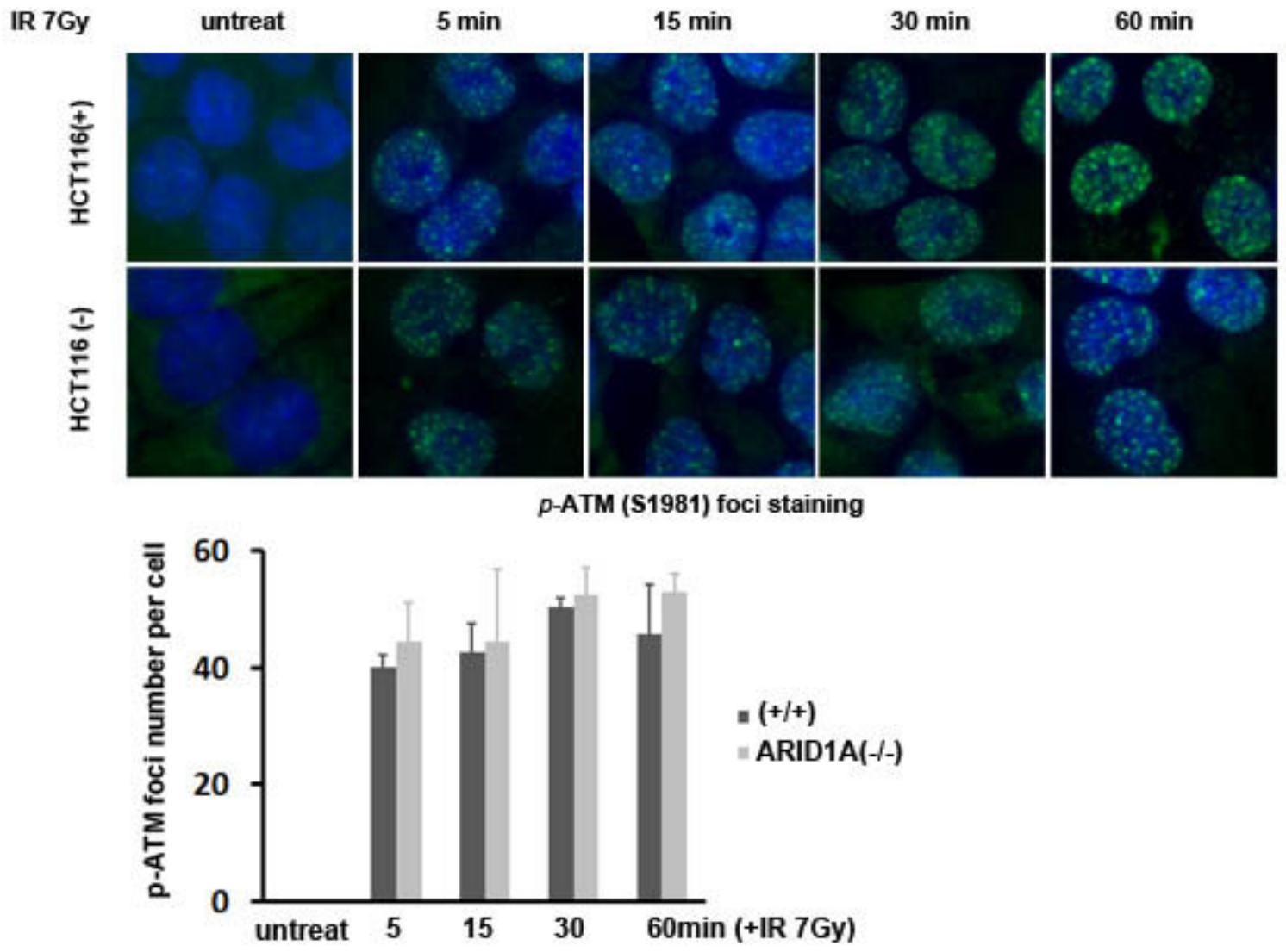
IR 7Gy
untreat
5 min
15 min
30 min
60 min
HCT116(+)
HCT116 (-)
p-ATM (S1981) foci staining
p-ATM foci number per cell
60
40
20
0
untreat
5
15
30
60min (+IR 7Gy)
(+/+)
ARID1A(-/-)

Figure S5

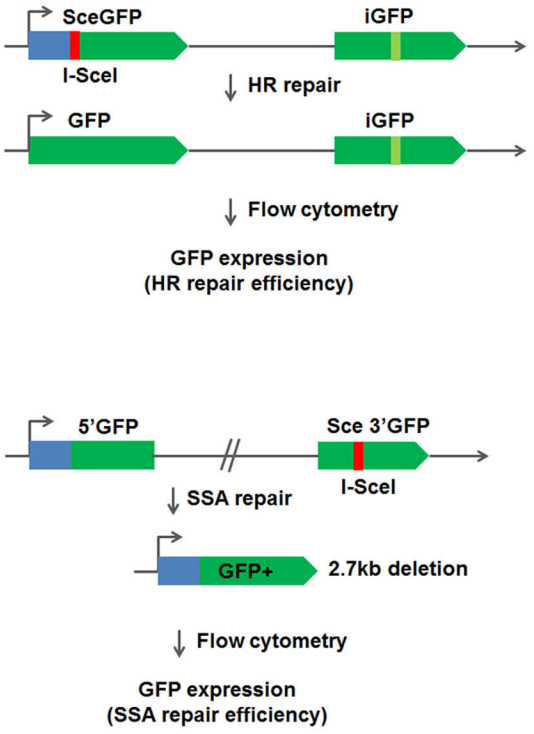
SceGFP
iGFP
I-SceI
HR repair
GFP
iGFP
Flow cytometry
GFP expression
(HR repair efficiency)
5'GFP
Sce 3'GFP
I-SceI
SSA repair
GFP+
2.7kb deletion
Flow cytometry
GFP expression
(SSA repair efficiency)

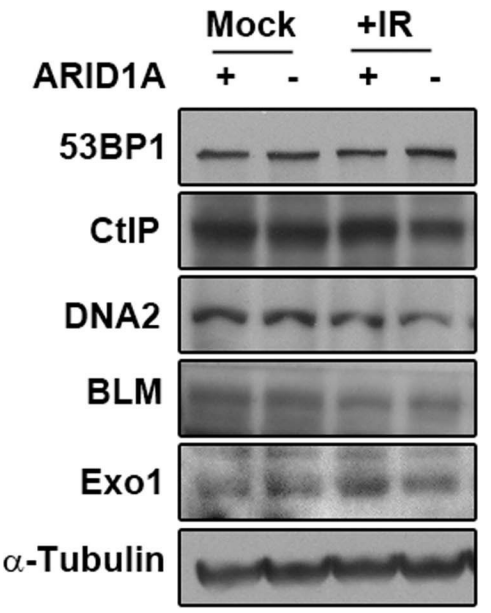
Mock
+IR
ARID1A
+
-
+
-
53BP1
CtIP
DNA2
BLM
Exo1
α-Tubulin

Figure S6

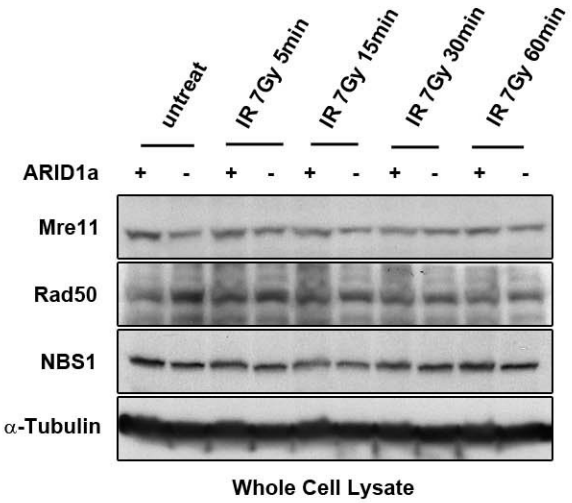
untreat
IR 7Gy 5min
IR 7Gy 15min
IR 7Gy 30min
IR 7Gy 60min
ARID1a + - + - + - + - + -
Mre11
Rad50
NBS1
α-Tubulin
Whole Cell Lysate

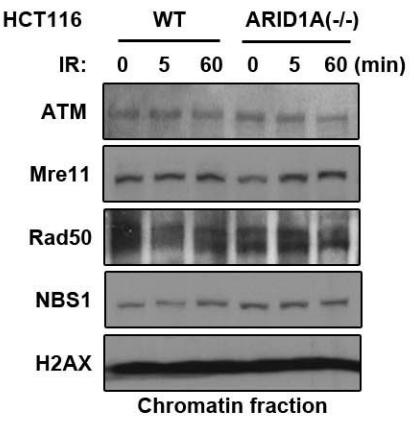
HCT116
WT
ARID1A(-/-)
IR: 0 5 60 0 5 60 (min)
ATM
Mre11
Rad50
NBS1
H2AX
Chromatin fraction